CERTL Reduces C16 Ceramide, Amyloid-β Levels and Inflammation in a Model of Alzheimer's Disease

Simone Mwenda Crivelli
University of Kentucky https://orcid.org/0000-0003-1776-7761
Qian Luo
Universiteit Maastricht School for Mental Health and Neuroscience
Jo Stevens
Universiteit Maastricht School for Mental Health and Neuroscience
Caterina Giovagnoni
Universiteit Maastricht School for Mental Health and Neuroscience
Daan van Kruining
Universiteit Maastricht School for Mental Health and Neuroscience
Gerard Bode
Universiteit Maastricht School for Mental Health and Neuroscience
Sandra den Hoedt
Erasmus Universiteit Rotterdam
Barbara Hobo
Nederlands Herseninstituut
Anna-Lena Scheithauer
Universitatsklinikum Bonn
Jochen Walter
Universitatsklinikum Bonn
Monique T Mulder
Erasmus Universiteit Rotterdam
Christopher Exley
Keele University
Michelle M. Mielke
Mayo Clinic Minnesota
Helga E De Vries
VU medisch centrum
Kristiaan Wouters
Universiteit Maastricht Cardiovascular Research Institute Maastricht
Daniel L.A. van den Hove
Universitatsklinikum Wurzburg
Dusan Berkes

Slovenska Technicka Univerzita

María Dolores Ledesma

Universidad Autonoma de Madrid Centro de Biologia Molecular Severo Ochoa

Joost Verhaagen

Nederlands Herseninstituut

Mario Losen

Universiteit Maastricht School for Mental Health and Neuroscience

Erhard Bieberich

University of Kentucky

Pilar Martinez-Martinez (p.martinez@maastrichtuniversity.nl)

https://orcid.org/0000-0002-5990-3373

Research article

Keywords: ceramide, sphingomyelin, ceramide transporter protein (CERT), adeno-associated virus (AAV), Alzheimer's disease (AD), 5xFAD,amyloid-β plaques, neuroinflammation, microglia

Posted Date: June 15th, 2020

DOI: https://doi.org/10.21203/rs.3.rs-33901/v1

Version of Record: A version of this preprint was published at Alzheimer's Research and Therapy on February 17th, 2021. See the published version at https://doi.org/10.1186/s13195-021-00780-0.

Abstract

Background: Deregulation of ceramide and sphingomyelinlevels have been suggested tocontribute tothe pathogenesis of Alzheimer's disease (AD).Ceramide transfer proteins (CERTs) are ceramide carriers, crucial for ceramide and sphingomyelin balance in cells.Extracellular forms of CERTs co-localize with amyloid-β (Aβ) plaques in AD brains. To date, the significance of these observations for the pathophysiology of AD remains uncertain.

Methods: The plasmid expressing $CERT_L$, the long isoform of CERTs, was used to study the interaction of $CERT_L$with amyloid precursor protein (APP) by co-immunoprecipitation and immunofluorescencein HEK cells.The recombinant $CERT_L$ protein wasemployed to study interaction of $CERT_L$with amyloid-β (Aβ), Aβ aggregation process in presence of $CERT_L$, and the resulting changes inAβ toxicity in neuroblastoma cells. $CERT_L$was overexpressed in neurons by adeno associatedvirus (AAV) in a familial mouse model of familial AD (5xFAD). Ten weeks after transduction animal were challenged with behavior tests for memory, anxiety and locomotion. At week twelve brains were investigated for sphingolipid levels by mass spectrometry, plaques and neuroinflammation by immunohistochemistry, gene expression and/or immunoassay.

Results:Here, we report that $CERT_L$, binds to APP, modifies Aβ aggregation and reduces Aβ neurotoxicity *in vitro*. Furthermore, we show that intracortical injection of AAV, mediating the expression of $CERT_L$, decreases levels of ceramide d18:1/16:0 and increases sphingomyelin levels in the brain of male transgenic mice, modelling familial AD (5xFAD). $CERT_L$*in vivo* over-expression hasa mild effect on animal locomotion and decreases Aβ formation and modulates microglia by decreasing their pro-inflammatory phenotype.

Conclusion: Our results demonstratea crucial role of $CERT_L$ in regulatingceramidelevels in the brain, in amyloid plaque formation and neuroinflammation,thereby opening research avenuesfor therapeutic targets of AD and other neurodegenerative diseases.

Background

Key pathologicalfeatures of Alzheimer's disease (AD) are aggregates of amyloid- β peptides (Aβ) andneurofibrillary tangles (NFTs),and neurodegeneration, together with blood-brain barrier (BBB) dysfunction, neuroinflammation and lipid disbalance. To date, the molecular mechanism underlying neurodegeneration in AD remains unclear. Elucidation of the deregulated biological mechanisms that lead to the onset and progression of AD is critical to identify new treatment strategies (1-5).

Sphingolipids (SLs) are waxy lipids formed by a sphingosine backbone, important for the cell membrane architecture and for the function of transmembrane proteins. Furthermore, SLs such as ceramides (Cer) and sphingosine-1-phosphate (S1P) are potent second messengersthat regulate various importantcellular processes,includingcell growth and apoptosis (6-9). Cerare formed by two metabolic pathways: *de novo*

synthesis initiated with the precursor palmitoyl-CoA or catabolism of complex SLssuch as sphingomyelin (SM) (10-12). In the cell membrane, SLs are typically organized in microdomains, called lipid rafts, characterized byspecific SLspecies composition.

Several studies have analyzed lipid composition in AD brain tissue,reportingan increaseof Cerspecies (13-16). Lipid rafts enriched inCer, isolated from postmortem frontal cortex tissueof AD postmortem tissue,patients showed a reduction of SM levels compared to those isolated from the control brains(17). Moreover, SM levels inbrain regions, particularly vulnerable to Aβ plaque formation were reduced in AD brains [19, 20].Strong evidence links Aβ pathology to SL homeostasis. The enzymesβ-secretase and γ-secretase, which cleave the amyloid precursor protein (APP) to generate Aβ, are stabilized and have an increased half-life in Cer enriched conditions, thus increasing Aβ biogenesis (18, 19). In turn, Aβ can stimulate Cerproduction by directly activating the phosphodiesterase enzyme sphingomyelinase which converts SM to Cer(20, 21).

Ceramide transfer proteins (CERTs) contain a steroidogenic acute regulatory protein (StAR)-related lipid transfer (START) domain that confers the ability to transport Cer intracellularly between the endoplasmic reticulum(ER) and the Golgi(22). CERTs are found in at least two isoforms,which differ for the presence of a 26-amino acid serine-rich domain(23). CERTs are expressed in the central nervous system, and they are crucial in embryogenesis and brain development (23-25). When CERTs' activity is blocked pharmacologically or genetically, by compromising the START domain of the protein, SM production decreases significantly (26, 27). $CERT_L$can be secreted extracellularly and was found to partially co-localizewith serum amyloid P component (SAP) and with amyloid plaques in AD brain(28, 29). Besides, CERTs are also potent activators of the classical complement pathway that plays an active role in AD pathogenesis (30).To date, the significance of these observations for the pathophysiology of AD remains uncertain.

In the current study, we investigated the interaction of $CERT_L$with APP and Aβ*in vitro*. Next, we explored the effect of $CERT_L$ overexpression on SLcomposition, amyloid formation, and inflammation *in vivo* using adeno associated virus (AAV)-mediated genedelivery in the 5xFAD mouse model (31). Our findings showed that an increase of $CERT_L$ modulatedSL levels byreducing specific Cer and elevating SM. Notably, $CERT_L$also affected amyloid plaque formation and brain inflammation, typical pathological hallmarks of AD,supporting the idea that enzymes and transporters of the SLpathways are at the core of the pathophysiological changes observed in AD.

Material And Methods

$CERT_L$ interaction with APP/Aβ

Immunoprecipitation (IP). Wild type HEK293 and transgenic HEK293cells that stably overexpress humanAPP695 isoform (NP_958817.1)(32), were cultured in DMEM supplemented with fetal bovine serum (FBS), Pen/Strep, and L-glutamine. Stable transfected HEK-APP were maintained in G418 selective

medium. Prior to the experiment, cells were seeded in 25 cm^2 flasks and maintained in serum-free DMEM for 24 hours. For the homogenization, cells were washed two times with PBS, collected in lysis buffer (25mM Tris HCl pH 7.5,150 mM NaCl, 0.5% Triton X-100 and protease inhibitors), centrifuged at 20,000x g for 30 minutes and the resultant supernatants collect for the protein Bradford analysis. Protein extracts (100µg)from HEK or HEK-APP were used for immunoprecipitation experiments. Pull down of endogenous $CERT_L$ and APP was performed with 1 µgmAb anti $CERT_L$ (3A1-C1) (28) and anti-Aβ mAb 6E10 (Covance), respectively by 1-hour incubation at room temperature. mAb anti syntaxin 6335 (clone 3D10, Abcam) was used as an isotype control. Next, anti-mouse secondary antibodies (Euroegentec) were used to pull down the immune complex. Thereafter, samples were centrifuged at 20,000xg for 30 minutes. Pellets were washed three times in 50 µL PBS and boiled in reducing sample buffer containing mercaptoethanol to solubilize immunocomplexes. Then, the proteins were separated on a Tris-HCl 4-15% gradient gel (Bio-Rad), and blotted on nitrocellulose membrane (Millipore). Next, the membranes were probed withanti-Aβ/APP(6E10)or rabbit pAb anti-CERTs (epitope 1-50 of human CERTs, Bethyl Laboratories) antibodies.After 3 washes, membranes were incubated with donkey anti-mouse IRdye 680 and goat anti-rabbit IRdye 800 (Rockland Immunochemicals) and scanned using the Odyssey infrared imaging system.

Immunofluorescent staining. HEK-APP cells were seeded into a 60 mm dish containing sterile glass coverslips for reattachment. Cells were then fixed with 3.7 % PFA in PBS at 37°C for 15 minutes washed three times with PBS and incubated with 0.5 % BSA. Cells were stained with polyclonal anti CERTs (epitope 130-218 of human CERTs, Sigma) and with a human mAb anti APP (28). Next, cells were analyzed using an inverted fluorescence microscope (Olympus IX-81) and photomicrographs were acquired using µManager software (33) with an EXi Aqua (QImaging) digital camera.

Microscale thermophoresis binding analysis. Microscale thermophoresis (MST) analysis was performed in the Monolith NT.155 instrument (Nanotemper). In brief, 20 nM of NT647 labeled CERT was incubated for 20 minutes at room temperature in the dark with different concentrations of either $Aβ_{1-42}$ (rPeptide Athens) (3-100,000 nM) or control 17kDa Lama antibody fragment (H6) (1-35,000 nM) in PBS Tween20 (0,01%). Afterward, 3-5 µL of the samples were loaded into glass capillaries (Monolith NT Capillaries, Cat#K002), and the thermophoresis analysis was performed (LED40.51%, IR laser 80%). Statistical analysis was performed with Origin8.5 Software.

Aβ aggregation assay and cell-based toxicity assay

Transmission Electron Microscopy (TEM).$Aβ_{1-42}$, purchased as the lyophilized salt (Bachem), was dissolved in 0.01M NaOH in ultrapure water to give an $Aβ_{1-42}$ stock solution of *ca* 0.20mM, which was used immediately to prepare each of the treatments. The remaining peptide stock solution was frozen at -20^oC until required. Under these highly alkaline conditions, the peptide is fully dissolved and exists only as monomers (34). Treatments containing $Aβ_{1-42}$ and / or $CERT_L$(28), were prepared in 0.20µm filtered modified Krebs-Henseleit (KH) medium (118.5mM NaCl, 4.8mM KCl, 1.2mM $MgSO_4$, 1.4mM $CaCl_2$, 11.0mM glucose), buffered in 100mM PIPES at pH 7.4, including 0.05% w/v sodium azide to inhibit

microbial growth. Treatments were incubated at 37 ^{o}C until their specified time points prior to being prepared onto TEM grids. For replicate treatments, $A\beta_{1-42}$was thawed thoroughly immediately before use and then vortexed briefly. The stock solution was centrifuged at 15,000 rpm for 5 minutes, and 2.0 µL was then taken ready for concentration determination by absorbance at 280 nm, utilizing a NanoDrop 1000 spectrophotometer (Thermo). A value of 1390 M^{-1} cm^{-1} was taken as the extinction coefficient for $A\beta_{1-42,}$ and the resultant concentration was calculated by the application of the Beer-Lambert law. $CERT_L$ concentrations were determined in the same manner with a value of 107925 M^{-1} cm^{-1} taken as the extinction coefficient using the 72 kDa recombinant $CERT_L$ sequence ($hCERT_L$, 1875bp NP_005704.1).

All samples for TEM were prepared via a modified TEM staining protocol(35). Pre-coated S162 200 mesh formvar / carbon coated copper grids (Agar Scientific), were inserted into 20.0µL of the treatment beaded onto paraffin film for 60 seconds, then wicked, passed through ultra-pure water, re-wicked and placed into 30µL 2% uranyl acetate (in 70% ethanol), for 30s. Following staining with uranyl acetate, grids were removed, wicked, passed through ultra-pure water, re-wicked, and placed into 30µL 30% ethanol for 30s. Grids were finally re-wicked following this step, covered and allowed to dry for up to 24h, prior to analysis via TEM.

Samples for TEM were viewed on a JEOL 1230 transmission electron microscope operated at 100.0 kV (spot size 1), equipped with a Megaview III digital camera from Soft Imaging Systems (SIS). Images were obtained on the iTEM universal TEM imaging platform software.

Aggregation assay. $A\beta_{1-42}$ was purchased from Anaspec. The peptide was solubilized in sterilized PBS, 0.1 % trifluoroacetic acid (TFA) at the concentration 2 mM and frozen in aliquots at -80°C. Aliquots were diluted at the final concentration of 20 µM in a total volume of 400 µL containing 1 or 2.5µM of affinity-purified recombinant $CERT_L$(28). Samples were kept under rotarod shacking for 1, 2, 4, 8, 12 and 24 hours at 37°C before adding 5 µL to 95µL of thioflavin T (ThT) concentrated 20 µM, dispensed in 96 well optical plate and measuring fluorescent excitation at 450 nm and emission 486 nm in Victor X3 plate reader (Perkin-Elmer). 15 µL of the samples were also loaded onto a precast TGX 4-16 % gel either under native non-reducing or denaturing reducing conditions. Samples were then transferred to nitrocellulose membrane, blocked with 5% BSA in PBS and probed with mouse mAb anti-$CERT_L$ (3A1-C1) and human mAbs against Aβ (20C2, 3D6 and m266) as previously described (28). After incubation with goat anti-rabbit IRdye 800 and donkey anti-mouse IRdye 680 (Rockland Immunochemicals) the membranes were washed and scanned with Odyssey imager Li-Cor.

Toxicity assay.SH-SY5Y cells were seeded on a 96-well plate at a density of 3×104 cells per well in 1:1 DMEM:F12 with phenol red, 4mM glutamine, 200U/ml penicillin, 200U/ml streptomycin, MEM non-essential amino acids (100×; Gibco) and 10% FBS, and incubated at 37°C for 24hours,reaching up to 100% confluency, with 5% CO_2.After 24 hours, the medium was removed and replaced with 100 µl/well medium without phenol-red, containing 2% FBS and with 10µM $A\beta_{1-42}$ oligomers, and/or 1µM $CERT_L$, or alone to control wells and incubated for 24 hours.10 µl of MTT (4 mg/ml) was added to each well and

incubated at 37°C for 3 hours. MTT solution was decanted and the formazan was extracted with 100 µl of 4:1 DMSO:EtOH. Plates were read at 570nm, with a reference filter at 690nm.

Generation of adeno-associates virus

Human collagen type IV alpha 3 binding protein cDNA sequence ($hCERT_L$, 1875bp NP_005704.1) was cloned into the plasmid AAV-6P-SEW a kind gift of Prof. S. Kugler Department of Neurology, University of Gottingen. The transgene expression was controlled by a human synapsin-1 promoter (hSYN, 480bp), and an internal ribosome entry site (IRES 566bp) enabled the co-expression of EGFP(36). The plasmid expressing exclusively EGFP was used as a control (pAAV-EGFP). The AAV-$CERT_L$ plasmid was sequenced by GATC Biotech laboratories and both AAVs plasmids were tested *in vitro* in our laboratories. AAVs particles were produced as explained previously (37). In brief, the transfer plasmidspAAV-EGFP or pAAV-$CERT_L$ were used to produce AAV2 particles. Eight 15-cm petridishes each containing 1.25x107 HEK 293T cells in Dulbecco's modified Eagle's medium (DMEM) containing 10% fetal calf serum (FCS) and 1% penicillin/streptomycin (PS; all GIBCO-Invitrogen Corp., New York, NY, USA) were prepared one day before transfection. The medium was refreshed 1 hour prior to transfection to Iscoves modified Eagle medium (IMEM) containing 10% FCS, 1% PS, and 1% Glutamine. Transfer plasmids were co-transfected using polyethylenimine (PEI, MV25000; Polysciences Inc.) in a ratio of 1:3 with the pAAV-EGFP or pAAV-$CERT_L$ resulting in a total amount of 50 µg of plasmid DNA per plate. The day after transfection, the medium was replaced with fresh IMEM with 10% FCS, 1% PS, and 1% Glutamine. Two days later (3 days post-transfection), cells were harvested in D-phosphate buffered saline (D-PBS, GIBCO) and lysed with 3 freeze-thaw cycles. Genomic DNA was digested by adding 10 µg/ml DNAseI (Roche Diagnostics GmbH) into the lysate and incubated for 1 hour at 37 °C. The crude lysate was cleared by ultracentrifugation at 4000rpm for 30 minutes. The virus was purified from the crude lysate using the iodixanol gradient method, diluted in D-PBS/5% sucrose and concentrated using an Amicon 100kDa MWCO Ultra-15 device (Millipore). All AAV vectors were stored at -80°C until use. Titers (genomic copies/ml) were determined by quantitative PCR on viral DNA primers directed against the EGFP portion (Forward: GTCTATATCATGGCCGACAA; Reverse: CTTGAAGTTCACCTTGATGC). The AAV particles produced with pAAV-$CERT_L$ are referred to in this paper as AAV-$CERT_L$ while the particles produced with pAAV-EGFP are named AAV-control.

Animals

In this study, male mice were used in the present study. To investigate transduction efficiency over time we employed 24 C57BL/6wild type (WT) animals. A detailed description of the timeline and the experimental design can be found in the supplementary Figure 1B. B6/SJL WT and 5xFAD animals were obtained from the Jackson Laboratory and bred in house using 5xFAD x non-carriers.This breeding strategy may breed out the retinal degeneration allele Pde6brd1 from the original strain. The Jackson Lab has observed a less robust amyloid phenotype in this strainThe 5xFAD model carries 5 familial AD

mutations, three of themin the human *APP* transgene (Swedish, Florida, and London), and two in the human presenilin-1 (*PS1*) transgene (M146L and L286V mutations). These mutations lead to an increase in Aβ peptide production(31).nimals were individually housed under a 12 h light/dark cycle in individually ventilated cages. One week before behavioral tests, animals were adjusted to a reversed day-night cycle. Food and water were provided ad libitum throughout the study. All experiments were approved by the Animal Welfare Committee of Maastricht University(project number DEC2013-056 and DEC2015-002) and followed the laws, rules, and guidelines of the Netherlands.

Stereotactic injection

The animals underwent bilateral stereotactic injections. Mice were placed in a stereotactic head frame, and after midline incision of the skin, two holes were drilled in the skull in the appropriate location using bregma and lambda as references. The layer V of the motor-sensory frontal cortex was targeted; this was verified by light microscopy to observe the dye. Coordinates were determined as follows: anterior-posterior [AP] 0.06; mediolateral [ML] +/- 0.15; dorsoventral [DV] -0.1 (38). The AAVs were injected at the dose of 1.12*10E8 transducing unit (t.u.) in the anesthetized mice at a rate of 0.2 µ l / minutes with a final volume of 1 µL for each side.

Behavioral procedures

TheOpen field (OF) task was performed as described elsewhere (39). Briefly, locomotion activity was assessed in a square divided into 4 equal arenas. At the start of a trial, the animals were placed in the center of each arena. The total distance traveled was measured under low light conditions by a video camera connected to a video tracking system (Ethovision Pro, Noldus).

The Y-maze spontaneous alternation (AYM) test was conducted to assess spatial working memory.Mice were placed randomly in one of the three arms of the Y-maze and were left free to explore the arena for 6 minutes. The number of arm entries and the number of triads were recorded in order to calculate the percentage of alternations to measure working memory.

The Elevated zero-maze (EZM) was used to measure anxiety. It consists of a circular runway which is divided equally into two opposite open and two opposite enclosed arms. The mice were placed into one of the open arms and allowed to explore the maze over a period of 5 minutes. Thetotal and relative duration (in %) and distance traveled in the open and enclosed arms were measured in the dark via an infrared video camera connected to a video tracking system (Ethovision Pro, Noldus). Percentage (%) of time spent in the open arms was corrected for latency to first closed arm entry.

The Y-maze spatial memory test (SYM) was performed using the same arena as described in AYM above. One arm of the arena was closed by a removable blockade placed in front of it. The mice were placed in one of the open arms, which was randomized over the groups and allowed to explore the 2 open arms of the maze for 5 minutes (pre-test). Afterward, the animal was taken from the arena and put back into its

home cage. Five hours later, the mouse was placed back into its corresponding start arm of the arena, now with all three arms accessible (post-test). The previously blocked arm was termed the “novel arm”. Memory was evaluated by calculating the amount of time spent in the novel armcorrected for the latency to move from the start arm to another arm and the amount of time the animal spent in the center of the maze (40).

Immunofluorescence staining

Mice were sacrificed by intracardial perfusion using Tyrode's solution for the first minute, followed by fixation solution 4% paraformaldehyde (PFA) for 10 minutes under deep sodium pentobarbital anesthesia (150 mg/kg). The brains were removed and post-fixated overnight in 4% PFA fixation solution, and subsequently moved every 24 hours in a buffer containing a gradually higher sucrose percentage: 10% and 20% sucrose in 0.1 M phosphate buffer solutions (PBS). Afterwards, brains were quickly frozen using CO_2 and dissected into 16 µm thick sagittal sections using a cryostat (at -25^{o}C; Leica). All series of sections were subsequently stored at -80°C until further processing. For the CERTS and neuron co-localization stain, we incubated the antibodies separately to reduce the antibody-antigen interaction. Before the antibodies incubation, the slice sections were fixed with acetone 10 min and blocked with 0.3% H2O2 for 1h. The sections were incubated with a monoclonal NeuN primary antibody(1:50, chemicon international Inc, Temecula, CA, USA) overnight at 4 ^{o}C. Sections were washed 3 times with TBS, TBST, and TBS and streptavidin Alexa 594 (1:500) applied for 1h at room temperature. Then rabbit polyclonal anti-CERTS (epitope 300-350, Bethyl Laboratories) diluted 1:250 was used for recognized CERTS antigen. After overnight incubation, and the corresponding secondary antibody Alexa Fluor- 647(1:100) was applied for 1h at RT. The slices were mounted and stored in 4^{o}C before taking pictures. Next immunofluorescence co-labeling was performed with either anti-Iba1 rabbit (Wako Pure Chemical Corporation) or anti-glial fibrillary acidic protein (GFAP) mouse combined with anti-Aβ plaques human antibodies(41). Subsequently, the corresponding anti-rabbit or anti-mouse and anti-human secondary antibodies conjugated to Alexa Fluor-594 or 488 (Jackson ImmunoReseach Laboratories) were added for 2 hours. Washeswere performed 3 times for 10 minutes in TBS with 0.2% Triton-X100 (TBS-T), TBS, and TBS-T, respectively in between the antibody incubation steps. Densitometric analysis of the stainings were performed on sagittal brain sections at different lateral depth (6-9 sections per animal) with ImageJ. Microglia ramification and sphericity were analyzed as previously described (42).

Sphingolipid analysis

*High pressure liquid chromatography-tandem mass spectrometry (HPLC-MS/MS).*Powder aliquots of cortex, hippocampus, and cerebellum tissue were homogenized in PBS at the concentration of 10µL /1mg. Then, 50µL of the brain preparation (or 25 µL of plasma) were used to measure Cer, sphinganine (SPA), sphingosine (SPH), sphingosine-1-phosphate (S1P) as previously described (43, 44). Briefly, brain preparation (or plasma) was spiked with internal standards mixture prior to undergoing extraction. Data

acquisition was done using select ion monitor (SRM) after chromatographic separation and electrosprayionization on the Thermo TSQ Quantum Ultra mass spectrometer (West Palm Beach) coupled with a Waters Acquity UPLC system (Milford) for Cer, sphinganine (SPA), sphingosine (SPH), sphingosine-1-phosphate (S1P). SM data acquisition was done using multiple reaction monitoring after chromatographic separation and electrospray ionization on the Sciex Qtrap 5500 quadruple mass spectrometer (AB Sciex Inc., Thornhill, Ontario, Canada) coupled with a Shimadzu HPLC system (Shimadzu, Kyoto, Japan). Concentrations of each analyte were calculated against each perspective calibration curve and corrected for internal standard concentrations.

Protein extraction

Mice were terminally anesthetized with sodium pentobarbital, perfused and the brain removed and dissected into cortex, hippocampus and cerebellumEach brain region was then powdered in iron mortar partly emerged in liquid nitrogen, and aliquoted. Frozen tissue from dissected brains was sonicated in about 15 volumes (w/v) of Tris buffer saline (TBS) with PhosSTOP and protein inhibitors (Roche). Samples were centrifuged, and the TBS-soluble fraction was aliquoted prior to freezing in liquid nitrogen and stored at −80 °C. The pellet was re-suspended in about 15 volumes of TBS buffer containing 1% Triton-X 100and protease inhibitor cocktail with sonicator 1 cycle for 20 seconds. Samples were centrifuged, and the TBS-T-soluble fraction was aliquoted and frozen as described for TBS. The pellet was re-suspended in 70% formic acid to 150 mg/ml based on tissue weight, and mixed by rotation at room temperature for 2 h. Samples were centrifuged, and the formic acid-soluble fraction was neutralized (with 20 volumes of 1 M Tris base), aliquoted, and frozen at −80 °C. Total protein content in the TBS and TBS-T extractions was determined with Bio-Rad DC(Life Science Group) protein assay following the manufacturer's instructions.

Aβ immunoassay and Western blot

Immunoassay.Microplates Microlon/F-shape REF 655092 (Greiner) were coated with 1 µg/mL of human 3D6 (28)overnight at room temperature in coating buffer (sodium carbonate pH=9.6 0.05M $NaCO_3$ in MQ water). After washing plates (washing buffer 0.05% Tween- 20 in PBS were blocked with 4% not fat dry milk and incubated with brain homogenates or with Aβto generate the standard curve. Next plates were washed, incubated with 50ng/mL of biotinylated human 20C2(28) and washed again. Finally, plates were incubated with streptavidin-HRP (Jackson ImmunoResearch Laboratories) diluted 1:8,000 and developed using 3,3',5,5'-Tetramethylbenzidine (TMB).The absorption was measured at 450 nm within 30 minutes of stopping the reaction with 2 M H_2SO_4 using the Perkin Elmer 2030 manager system.

Western blot. TBS and TBS-T samples corresponding to 40 µg of total protein we loaded onto a precast TGX 4-16% gel (Bio-Rad). Then samples were transferred to PDVF membranes, blocked with Odyssey blocking buffer and probed with 1µg mAb anti-Aβ (6E10, Covance). After incubation with donkey anti-mouse IRdye680 (Rockland Immunochemicals) diluted 1:1,000 in Odyssey blocking buffer, the membrane

was scanned and analyzed with Odyssey imager Li-Cor. The intensities of the APP bands detected at 100 kDa, were measured with Odyssey imager Li-Cor.

Reverse transcription polymerase chain reaction (RT-PCR)

Total RNA was isolated from 20-50 mg of cortex using Trizol reagent (Invitrogen). One microgram of total RNA was treated with DNAse I and transcribed into cDNA (Superscript III, Invitrogen). PCR was performed in duplicate withSensiMix™ SYBR® Low-ROX Kit (Bioline) using the set of primers reported in supplementary table 1. Fold changes of expression relative to control were determined after normalization to GAPDH and Actin. Fold change was calculated by the comparative Ct method (45).

Statistical analysis

Statistical analysis was performed using the Statistical Package for the Social Sciences (SPSS 23.0 SPSS Inc., Chicago, IL, USA). All graphs were designed in GraphPad Prism (version 5,GraphPad Software, San Diego, CA, USA).All data shown are expressed as mean ± standard error of the mean (SEM). Behavioral tasks, SLs, RT-PCR and cytokines data were analyzed with two-way analysis of variances (ANOVA) with AAV treatment and genotype as independent factors. Least Significant Difference (LSD) was used for *post-hoc* testing. Comparison of mean values from two groups were performed by an unpaired two-tailed Student's *t*-test or by Mann–Whitney U test for non-parametric testing. P-Values were considered as significant if $p \leq 0.05$ and marked with (*). Results were marked with (**) if $p \leq 0.01$, or (***) if $p \leq 0.001$.

Results

$CERT_L$ directly affects Aβ aggregation and toxicity *in vitro*.It has been demonstrated that specific forms of CERTs can be released extracellularly or found membrane bound(29). We have shown that CERTs can be found in proximity to Aβ plaques in AD brain, where they partially co-localize with SAP and with amyloid fibrils(28). Here,we tested whetherthe long isoform of CERT, $CERT_L$, interacts with Aβ and its precursor protein APP.Cellular extracts of HEK-APP, expressing endogenous $CERT_L$,and stably expressing APPwere incubated with monoclonal antibodies (mAbs) against $CERT_L$, APP and syntaxin 6(used as a negative control) for immunoprecipitation (IP). Pull downwas performed with anti-mouse antibodies for all 3 conditions as explained in material and method section. Western blot analysis of the samples showed efficient IP of $CERT_L$ and APPby their respective antibodies. APP was detected as a band around 100 kDa whereas $CERT_L$was detected as a band of 200 kDa. The two respective bands were visualized either when $CERT_L$ or APP werepulled down, but not when syntaxin 6 was used instead.The results, representative of three independent experiments, showed an interaction between $CERT_L$ and APP(Figure 1A). The two proteins show partial colocalization in HEK-APP cells at the plasma membrane and in the perinuclear region (Figure 1B). As shown by microscale thermophoresis (MST) analysis, $CERT_L$also binds to $A\beta_{1-}$

$_{42}$(K_d=2.5μM) (Figure 1C)and byWestern blot (Supplementary figure 1A, B). Having shown that $CERT_L$ directly binds to APP and Aβ, we next tested whether binding of $CERT_L$ to $Aβ_{1-42}$ could directly influence the spontaneous fibrilization of $Aβ_{1-42}$by ThT fluorescence spectrometry and TEM. In the absence of $CERT_L$, the thioflavin T (ThT) fluorescence of $Aβ_{1-42}$ peaked after 10-12 hours indicating amyloid formation.With the addition of $CERT_L$ (2.5 μM) $Aβ_{1-42}$ maximum ThT fluorescence reduced to 50%. In contrast, at 1 μM concentration, $CERT_L$ was ineffective at preventing $Aβ_{1-42}$ fibrilization (Figure 1D).

In addition to ThT fluorescence assay, we studiedAβ aggregation in the presence of $CERT_L$ by TEM.The TEM images showed that amyloid-like fibrils were observed in both conditions with and without $CERT_L$ in combination with Aβ. However, the amyloid structure identified in the presence of $CERT_L$was not linear in shape and the fibril width varied significantly (Figure 1E-F) when compared to $Aβ_{1-42}$alone. The aggregates observed with $CERT_L$ plus$Aβ_{1-42}$ could be precursors to amyloid fibril formation, but not classic straight amyloid fibril formation as previously reported (46).

Furthermore, using SHSY-5Y cells, we examined the effect of $CERT_L$ on cell viability when$Aβ_{1-42}$was present. The addition of oligomeric $Aβ_{1-42}$ to the culture medium of SHSY-5Y cells resulted in a 38% decrease in viability after 24 hours, as measured by MTT reduction relative to control conditions ($p<0.01$). Interestingly, the simultaneous addition of $CERT_L$ significantly ameliorated the toxic effect of $Aβ_{1-42}$ (Figure 1G). Our results indicate that $CERT_L$forms complexes with APP and Aβ. The interaction of $CERT_L$withAβ affected spontaneous aggregation and toxicity of the peptide.

As aforementioned, CERTs are important regulators of cellular Cer and SM balance. For this reason, we investigated the effect of modulating $CERT_L$ levels on SL composition *in vitro*. After 72-hour cell transfection with pcDNA3.1 carrying $CERT_L$,SM d18:1/16:0, SM d18:1/20:0 and SM d18:1/22:0were significantly increased while Cer were unchanged (Figure 1H).Furthermore, $CERT_L$ overexpression did not affect cell viability (data not shown).

Ceramide species are increased in 5xFAD compared to WT animals depending on brain region and acyl chain length. The 5xFAD model carries 5 familial AD mutations. These mutations lead to a rapid increase of Aβ peptide production. By 6 weeks of age, mice display elevated levels of Aβ, amyloid deposits, and age-dependent amyloid pathology accompanied by increase of inflammatory marker levels in the CNS (47-50). However, it is unknown if this model shows also an increase of Cer level in the brain as it has been reported in the brains of AD patient(13-16). Sphingolipid species were determined with HPLC-MS/MS in cortex, hippocampus and cerebellum of 5xFAD and wild type (WT) malemice at 25-26 weeks of age(Supplementary Table 1 reports complete analysis). The analysis showed a significant elevation of Cer d18:1/16:0 levelsin the cortex and of sphinganine (SPA), S1P, Cerd18:1/16:0, Cerd18:1/18:1, Cer 18:d1/20:0 andCerd18:1/22:0in the hippocampus of the 5xFAD animals compared to WT mice (Figure 2A and B). In the cerebellum only S1P levels were found to be significantly higher in the 5xFAD animals. These results indicate that at that specific age and disease stage of the animals the cortex and the hippocampus are more susceptible to increase of Cerlevelswhile the cerebellum is less affected. This

suggests that the increase ofCerlevels correlate with amyloid burden. In fact, the cortex and hippocampus are the areas where the plaques are firstreported to appear in this model (31).Quantification ofCERT levels in the cortex by immunoassay showed a significant reduction of the protein concentration in AD brains compared to controlsat 25-26 weeks of age(51).CERTs reduction was not observed in cerebellum (Figure 2D). Our data suggest that SL metabolism is shifted towards increased production of Cer at different degrees depending on the brain region. Furthermore, CERT concentration is reduced in the cortex of 5xFAD mice compared to WT.

AAV-mediated neuronal expression of $CERT_L$ in mouse brain. To test the hypothesis that increasing $CERT_L$ levels in the cortexcounteract the SL disbalance in 5xFAD animals andAβ formation, we generated AAV2 particles carrying the $CERT_L$cDNA sequence controlled by the neuron-specific synapsin promoter (Figure 3A). The AAV- $CERT_L$ was tested *in vitro* on cortical rat primary cell culture, proving to effectively transduce neurons (Supplementary figure 2A). Next, 8 weeks old WT animals were injected in the layer V of the motor cortex with AAV-$CERT_L$ and AAV-control(Supplementary figure 2B).Layer V of the frontal cortex was targeted since the Aβ accumulation is the most severe(31)and CERT levels are reduced in this mouse model. The transduction efficiency was evaluated 1-, 2-, 6- and 12-weeks post-injection by immunohistochemistry (Supplementary figure 1C-D)andby RT-PCR (Supplementary figure 1E). The AAV-$CERT_L$was shownto effectively transduce neuronal cells and expressed the $CERT_L$proteinfor at least 12 weeks.The AAVs were then injected in 5xFAD mice in a similar fashion. After 12 weeks CERT overexpression was confirmed by immunohistochemistry (Figure 3B) andby Western blot analysis (Figure 3C and D). The immunolabeling of CERT,with neuronal marker NeuN,showed as expected neuronal expression andthat AAV-$CERT_L$was injected in the targeted area of the cortex. The fluorescent immunolabeling of CERT also showed increased signal extracellularly. This suggests that AAV-$CERT_L$ increased the extracellular release of $CERT_L$ as well. Relative quantification of CERTs levels in cortex homogenatesby Western blot illustrated a significant increase of CERTs levels in AAV-$CERT_L$treated groups (Figure 3D).

5XFAD and WT mice injected with AAV-$CERT_L$and AAV-WTdid not show behavioral abnormalities.Mice underwent stereotactic surgery for CNS administration of AAV particles at 12-13 weeks of age and were monitored for 12 weeks. As mentioned above,AAVs were injected in layer V of the cortex. At week 10 post-injection, mice were challenged with a behavioral test battery in the following sequence: open field (OF) for assessing locomotion activity, Y-maze spontaneous alternation (AYM,) and SYM for assessing spatial memory and elevated zero-maze (EZM) for examining anxiety (Figure 4A-E). It has been reported that 5xFAD mice exhibit changes in hippocampus-dependent spatial working memoryby 16 to 24 weeks of age(31). However,in our hands, no differencewas found in the performance of 5xFAD compared to WT in locomotion (Figure 4B), memory (Figure 4C and E),) and anxiety (Figure 4D).Our data shows that the WT animals treated with the control virus performed above the 50% chance level in the AYM (Figure4C). Furthermore,in the OF,the AAV-$CERT_L$ attenuated 5xFAD hyperactivity, even though 5xFAD treated with AAV-control did not perform significantly different from WT animals (Figure 4B, two-way ANOVA,

interaction F=4.170, p=0.0463).Overall, these data suggest that no detrimental behavioral effectsin the animals wereobservedafter$CERT_L$over-expression.

AAV-$CERT_L$ decreased Cer d18:1/16:0and increased SM levels in the cortex.One of the main functions of CERTs is to shuttle Cerfrom the ER to the Golgi (22). It has been reported that toxic increase ofCer species in the muscle can be attenuated by overexpressing hCERTcDNA(52).HPLC-MS/MS analysis of brain cortex tissuerevealed a significant reduction of Cerd18:1/16:0 level due to $CERT_L$ overexpression ($p<0.05$). This effect was not observed in WT animals but only in 5xFAD animals where Cerd18:1/16:0 level was significantly elevated ($p<0.01$). This transport of Certo the Golgi is crucial for the *de novo* synthesis of more complex SLssuch as SM. Previous data from *in vitro* experiments reported that blocking CERTs function SM levels would significantlydecrease (26). Hence, if CERTs activity is enhanced, we expected an increase inSM levels. As reported above,we found that*in vitro* overexpression of $CERT_L$increasedthe levels of certain species of SM.Accordingly, SLanalysis of the cortex showed that the levels of most of SM species (SM d18:1/16:0 $p<0.001$, SM d18:1/18:0 $p<0.001$, SM d18:1/18:1 $p<0.01$, SM d18:1/20:0 $p<0.05$, SM d18:1/22:0 $p<0.05$ and SM d18:1/24:1 $p<0.01$) were increased in AAV- $CERT_L$ treated animals (Figure 5). The only SM species not found significantly elevatedwas the SM d18:1/24:0, whose precursor Cerd18:1/24:0 has been reported to be poorly transferred by CERTs (53).

These data suggest that $CERT_L$ overexpression is effective in reducing Cer increase by intensifying the transfer to the Golgi,which leads to an increase of SM. While the Cer attenuation was restricted to a pathological increase of Cerd18:1/16:0 level, SM elevation was consistent in all AAV-$CERT_L$ treated animals. This shift in SL composition did not affect apoptosis markers in the cortex quantified by RT-PCR (Supplementary figure 6A).

AAV-$CERT_L$ reduces Aβ levels by decreasing APP cleavage in the cortex of 5xFAD mice. Since our previous data indicated that $CERT_L$could be released to the extracellular milieu and directly affects Aβ aggregation and toxicity *in vitro*, we investigated the effect of $CERT_L$overexpression on Aβdeposition. (Figure 6 A). Statistical analysis showed no significant difference in plaque load between the 5xFAD groups at 24-26 weeks of age(Figure 6B). However, the percentage of small plaques size (10-25 μm) was reduced ($p<0.05$) inAAV-$CERT_L$treated 5xFAD brains (Figure 6 C). Furthermore, Aβ quantification of brain homogenate in TBS soluble and TBS-T soluble fraction showed that Aβ levels were reduced in samples treated with AAV-$CERT_L$ ($p=0.04$ and $p=0.03$, respectively), while in the formic acid soluble fraction no change was observed ($p=0.29$) (Figure 6 D). Since it has been reported that APP cleavage can be affected by Cer composition (18, 19), we investigated if the reduction of Cer and increase of SM levels mediated by AAV-$CERT_L$ is associated with altered processing of APP. The ratioAβ/ FL-APP was decreased in $CERT_L$ overexpressing mice implying a reduction of Aβ biogenesis or increase clearance of Aβ($p<0.01$). Since the CTFβ is the product of β-secretase cleavage of APP and the immediate precursor of Aβformation(54), the ratio of CTFβ / FL-APP bands intensities was used to assess APP processing by β- and γ-secretase. The CTFβ / FL-APP was found an increase in AAV-$CERT_L$ treated 5xFAD animals ($p<0.05$) (Figure 6 E). Meanwhile, the ratio Aβ/CTFβwas reduced in brains of $CERT_L$overexpressing mice ($p<0.01$)(Figure 6E and

Supplementary Figure 5). These results are indicative suggest that AAV-CERT$_L$affects the proteolytic processing of APP by β- and/or γ-secretase.

These results show that a specific balance of Cer to SMand/or interaction of CERT$_L$ with APP is critical for APP cleavage and Aβ biogenesis.

Four weeks of administration of CERTs inhibitor (HPA-12) exacerbatesCer andAβ pathology in AD transgenic mice. To test if efficient ceramide trafficking from the ER to the Golgi is vital in the regulation of the Cerlevels and Aβformation, we administeredthe CERTs inhibitor N-(3-hydroxy-1-hydroxymethyl-3-phenylpropyl) dodecanamide (HPA-12) for 4 weeks to AD transgenic mice. As expected Cer d18:1/16:0, Cer d18:1/20:0, Cer d18:1/22:0 and Cer d18:1/24:1 levels werefound an increase in the brain (Figure 7 A). Moreover,Aβ levels were increased by117% in the TBSsoluble fraction ($p<0.05$) and by 47% in the TBS-T soluble fraction of brain homogenates (*$p<0.05$)of CERTs inhibitor-treated AD animals. No significant changes were found in the FA insoluble fraction (Figure 7 B).

These data suggest that efficient ceramide transfer from ER to *trans*-Golgi, is critical to control Cerlevels and thereafter APP processing. Pharmacogical interference with CERT activity augments Cer levelsandincreases substantially Aβ biogenesis and/or fibrillization

AAV-CERT$_L$ reduces microglia immunoreactivity as shown by Iba1 labelingand CD86 expression. We have observed that CERTsare associated to Aβ plaques in AD brainwhere microglia cells areengaged(28). Thus, we investigated if microglia cells were affected by CERT$_L$ overexpression in the cortex**.** To achieve this aim**,** brain sections were analyzed for Iba1 reactivity. AAV-CERT$_L$ treated brains had a decreased immunoreactivity to Iba1 (percentage of area $p<0.001$) (Figure 8A-C). Iba1 is considered a constitutive marker for microglia, which is highly increased in 5xFAD animals compared to WT (55, 56). Furthermore, it has been shown to be important for membrane ruffling, a process crucial for macrophages and microglia motility and chemotaxis (57).We further characterized microglia based onramifications and sphericity. The analysis showed that microglia of AAV-CERT$_L$ injected mice had longer ramifications and lower sphericity index (Figure 8D and E). To investigate if AAV-CERT$_L$ affected other microglia membrane markers, we run RT-PCR on cortex tissue. We quantified the CD86membrane marker,whichis an indicator for microglia pro-inflammatorypolarization. Statistical analysis showed that CD86 was increased in AAV-control treated 5xFAD animals compared to AAV-control treated WTs, and that AAV-CERT$_L$ specifically decreases CD86 in the 5xFAD group (Figure 8F).

Next, we analyzed cytokines levels in brain homogenate usingmultiplex technology. The assay did not reveal any significant effect of AAV-CERT$_L$ treatment. However, we observed a significant increment of IL-1β ($p<0.01$) and a significant reduction of IL-4 ($p<0.05$) when comparing WT to 5xFAD animals in AAV-control treated groups (Supplementary figure 6A).

These results indicate overall that AAV-CERT$_L$decreasespro-inflammatory processes in microglia.

AAV-CERT$_L$ does not change the immunoreactivity of astrocytesas shown by GFAP labelingin the cortex of 5xFAD mice.Reactive astrocytes have been described as a pathological hallmarkthat generally occurs in response to neurodegeneration in AD (58). To determine the extent of astrocytosis in the 5xFAD mouse brain treated with AAV-CERT$_L$ compared to control, we performed immunofluorescenceGFAPlabelingon sagittal brain sections (Figure 8G). Densitometric and particle analysis performed with ImageJ did show a reduction of 47% astrocytes immunoreactivity, which was not statistically significant (Figure 6H).However, as previously reported we observed a 3 fold increase of GFAP immunoreactivity in the 5xFAD animals compared to WT controls (31, 59).

Discussion

In this work, we provide evidence suggesting that CERT$_L$ plays an important role in characteristic processes of AD by affecting Aβproduction and aggregation, neuroinflammationand SL disbalance typical of AD. Our data show that the pathological increase of Cer d18:1/16:0can be restored to normal levels by upregulating CERT$_L$.The reduction of Cerlevels also provedto beeffective in attenuating Aβformation. Furthermore, CERT$_L$overexpression in neurons revealed that CERT$_L$ can downregulate membrane markers indicating a pro-inflammatory status in microglia.

It has previously been reported that APP can interact with extracellular matrix proteins like collagen I (60, 61). This interaction is thought to be important in neuronal cell to cell adhesion with APP functioning as an anchor(62). CERT$_L$ is known to be crucial in stabilizing the basal membrane(63). We previously reported that CERTs can be found in close location to plaques in AD brains, where they co-localize with amyloid fibrils(28).In line with this, we found thatAPP can interact withCERT$_L$and form complexes that can be immune-precipitated.Also Aβcan bind to a variety of biomolecules, including lipids, proteins and proteoglycans(64). Here, we show that CERT$_L$binds directly to Aβ peptides andthat this interaction affects Aβ fibrilization by organizing Aβ into less neurotoxic aggregates.

Manipulation of CNS SL metabolism can be challenging. Removal or addition of genesin the SL pathway can be deleterious for brain function(65, 66). Also, the upregulation of specific enzymes in specific cell types can be harmful for brain function.In a previous report on SL interference by AAV particles delivering human acid sphingomyelinase in the brain of rodents and primates,showed that motor function could be severely affected(67). On the contrary, in our study,behavioral testing at 9-10 weeks post AAV particle injection revealed no detectable side effects when comparing AAV-CERT$_L$ to AAV-control treated animals in the various locomotor-, memory- and anxiety-related behavioral tasks. Of note though, we found a significant reduction of locomotor activity in the 5xFAD due to AAV-CERT$_L$ treatment. It has been reported that 5xFAD animals exhibit a hyperactive behavior compared to control animals even though this specific behavior is not utterly understood and translation to human symptoms is unclear (68). However, the question whether AAV-CERT$_L$ could improve memory or other behavioral deficits observed in the 5xFAD model could not be answered by our data. No significant impairments in spatial memory were detected in the AYM and the SYM tests. Jawhar et al., reported deficits of working memory, assessed by a cross-

maze test, to appear at 6 months (69). However, in the present study, none of the groups tested performed above chance level indicating lack of recognition in all groups examined. As such, future studies should additionally assess shorter inter-trial intervals in this respect.

Cergeneration is abnormalin AD, causing an increase in Cer formation(15, 70). Furthermore, an accumulating body of evidence consistently reported a global rise inCer levels in specific brain regions of AD patients(13, 71, 72). In agreement with these observations, we found that 5xFAD transgenic mice at 6 months of age also showed an increase of Cer d18:1/16:0 in the cortex and ofseveral Cerspecies in the hippocampus (Cer d18:1/16:0, Cer d18:1/18:1, Cer d18:1/20:0 andCer d18:1/22:0).Previously, other studies showed increased brain Cer levels indifferenttransgenic AD models (APP, PS1, and PS1-APP mutated mice)(73).This suggests that there is a causal relationship between amyloid pathology and Cer imbalance.

In a genome-wide gene-expression analysis on several? AD models, CERTs expression was found downregulated in the cortex compared to control (51). The deficient transfer of Cer from the ER to the Golgi implicates that Cer accumulates in the ER, causing a chronic stress-like reaction in the cell that compromises the unfolded protein response (UPR) pathway [10].In contrast, the enzymes of the SL catabolic pathway like sphingomyelinase are abnormally activecontributing to the Cer build-upin other cell compartments(15, 70). Cer accumulation contributesto amyloid pathology via two mechanisms:first, Cer increases Aβ production by stabilizing secretases activity; second, Aβ activates the Cer mediated apoptotic pathway (18, 19).

In this study we report that increasingCer trafficking from the ER to the Golgi by overexpressing $CERT_L$, reversed the pathological increaseof Cer in the cortex. A similar effect of CERTs overexpression in Cer elevation state has been reported in alipotoxic mousemodel where muscle cells in overload Cer statuswere rescued by increasing the expression of hCERT(52). In AD brains, we observed that $CERT_L$ reduced 11% of the total Cer content restoring it close to normal levels. In particular, Cer d18:1/16:0 was the most affected species by AAV-$CERT_L$being reduced up to 35%. These results demonstrate the importance ofphysiological ER-to-Golgi Cer traffic in preserving the physiological balance of Cer levels in ADpathology.

The solubleAβ formswere reduced in the $CERT_L$ treated animals, whereas the insoluble Aβ forms were not altered by the treatment. This reduction in the soluble forms could be explained in two ways: i) the11% reduction of total Cer due $CERT_L$ overexpression and ii) $CERT_L$ interaction with Aβ. As aforementioned, the amyloidogenic cleavage of APP is favored resulting in more Aβ formation in Cer enriched conditions(18, 19).In our study, the total Cer reduction may have affected the secretases activity in the opposite way. We found that the Aβ / APP ratio, which describes the APP processing to form Aβ, waslower in AAV-$CERT_L$ animals implying that lesserAPP is processed to generate theAβpeptide. Importantly, APP processing takes place in different cell compartments not only on the cell surface (74) and the Cer shift is not confined to the ER compartment but can affect the whole cell (75, 76). Thisconclusion was further confirmed by pharmacological inhibition of CERT Cer transfer activity with CERT inhibitorHPA-12.

Recently, the pharmacokinetics of HPA-12was described,and it was proven that the compound reaches the brain intact(24). Here, we found that after 4 weeks,the treatment of HPA-12 increases Cer andAβ levels.

It is now thought that one of the crucial processes in the development and exacerbation of AD is neuroinflammation(77). Genome-wide association studies reported that variants of genes encoding for immune system proteins, like triggering receptor expressed on myeloid cells 2 (TREM2), were discovered to be associated with AD pathophysiology(78). Additionally, different inflammatory markers such as activated astrocytes and microglia, increased levels of cytokines and products of complement (C) activation are found in the brain tissue of AD patients(79-82). This pro-inflammatory environment is thought to be harmful to neurons. As we previously reported, $CERT_L$also has immune functions. Our lab demonstrated that $CERT_L$ interacts with SAP which belongs to the pentraxin family of the innate immune system [34]. Additionally, we reported that $CERT_L$ can activate the complement system [33]. Here, we found that AAV-$CERT_L$ influenced microglia activation even though $CERT_L$ was specifically expressed in neurons under the control of the synapsin promoter. It has been consistently reported that 5xFAD microglia are polarized towards a more pro-inflammatory status, in response to the extensive plaque formation. Consequently, the Iba1 microglia marker is highly expressed in AD models [52, 53]. Our findings suggest that$CERT_L$could play a role in the cross-talk between neurons and microglia. Interestingly, neuronal-derived $CERT_L$activityis exerted only when there is an inflammatory reaction ongoing by reducing membrane markers for the pro/inflammatory status of microglia. Nevertheless, it remains unclear by which mechanism AAV-$CERT_L$decreases Iba1 and CD86 positive cells. Here, we propose two hypotheses. First, the reduction of Iba1 and CD86 is a direct action of $CERT_L$ on microglia activation status once secreted by neurons. It is known that forms of $CERT_L$ can be released in the extracellular space [58].The second, Iba1 and CD86 are decreased because of a modified by shifts in Cer and SM composition or other indirect effects like reduction of Aβ levels. In the CNS, there is an extensive cross-talk ongoing between neurons and microglia, which takes advantage of lipid vesicles. Furthermore,toxic Aβ hasalso been reported among the content of exosomeand reduction of exosome secretion was correlated to Aβ reduction (83, 84).

Similarly, to microglia,also astrocyte activationwasreduced by AAV-$CERT_L$, even though not significantly. During inflammation astrocytes are enriched in Cer. They seem to produce the pro-apoptotic Cer d18:1/16:0(85, 86). Further, reactive astrocytes release extracellular vesicle enriched in ceramide that carryAβ peptides(86).These specific extracellular vesiclesisolated from brains of 5xFAD mice showed to be particularly toxic for neurons.

Conclusion

In conclusion,by increasing $CERT_L$ expression in neuronal cells, we were able to increase SM production in the CNS. Next, after proving that $CERT_L$ binds and modifies Aβ aggregation *in vitro*, we observed that administration of AAV-$CERT_L$in AD animals reduced Aβ production by at least 2 mechanisms:by altering

SL composition andbydirect interaction with APPin 5xFAD animals. Moreover, we reporteda new immune role of $CERT_L$. AAV-$CERT_L$ decreased membrane markers important for the pro/inflammatory status of microglia. Overall, our experiments are the first to demonstrate that an increase of $CERT_L$, modulatesSL levels, affects amyloid plaque formation and brain inflammation in AD (see the model in figure 9). These data open research pathways for therapeutic targets of AD and related neurodegenerative diseases.

List Of Abbreviations

Alzheimer's disease	AD
Amyloid- β peptides	Aβ
Neurofibrillary Tangles	NFTs
Blood Brain Barrier	BBB
Sphingolipids	SLs
Ceramide	Cer
sphingosine-1-phosphate	S1P
Sphingomyelin	SM
Ceramide transfer proteins	CERTs
Ceramide transfer proteins long form	$CERT_L$
Steroidogenic acute regulatory protein (StAR)-related lipid transfer	START
Endoplasmic Reticulum	ER
Adeno associated virus	AAV
Immunoprecipitation	IP
Amyloid precursor protein	APP
Full length Amyloid precursor protein	FL-APP
C-terminal fragment-β	CTFβ
Microscale thermophoresis	MST
Transmission Electron Microscopy	TEM
Thioflavin T	ThT
Open field	OF
Y-maze spontaneous alternation	AYM
Elevated zero-maze	EZM
Y-maze spatial memory test	SYM
High pressure liquid chromatography-tandem mass spectrometry	HPLC-MS/MS
Monoclonal antibodies	(mAbs)
N-(3-hydroxy-1-hydroxymethyl-3-phenylpropyl) dodecanamide	(HPA-12)

Declarations

Ethics approval and consent to participate

All experiments were approved by the Animal Welfare Committee of Maastricht University (project number DEC2013-056 and DEC2015-002) and followed the laws, rules, and guidelines of the Netherlands.

Consent for publication

Not applicable

Availability of data and materials

The datasets used and/or analysed during the current study are available from thecorresponding author on reasonable request.

Competing interests

The authors declare that they have no competing interests.

Funding

This work was supported by grants to NMdW, SdH, MTM, JW, AR, PMM, and HEV from ZonMw Memorabel program (projectnr: 733050105) and to JV (Memorabel program grant, project number 7330598117). PMM is also supported by the International Foundation for Alzheimer Research (ISAO) (projectnr: 14545). SMC received a travel grant support from Alzheimer Nederlands foundation (AN) to spend a month in the laboratory of EB, University of Kentucky, Lexington KY, USA. Aspects of this work were supported by the grant NIH R01AG034389, R01NS095215, and R56AG064234; VA I01BX003643 to EB. MMM was supported by R01AG049704.

Authors` contributions

PM and ML conceived the project. PM, ML, SMC, QL, CG, JS, DVK, and GB designed and performed the animal behavior, biochemical and molecular biological experiments with critical input fromML, DVH, HEV, LDM and PM. JV and BH generated the adeno-associated virus particles. CH performed the electron microscopy. MM, MTM and SVH performed lipid mass spectrometry analyses. ALS and JW analyzed APP processing, contributed important reagents and cell models. DB synthesized and provided the CERTs inhibitor. BE helped to perform and interpreted the cytokine measurements in the brain homogenate. WK helped experiment design and data interpretation of neuroinflammation. The manuscript was written by SMC and PM. All authors contributed by critical revising the manuscript.

Acknowledgements

We thank a kind gift of Prof. S. Kugler Department of Neurology, University of Gottingen for the kind gift of adeno-associated virus plasmid. We thank Geertjan van Zonneveld for the professional approach and dedication to complete the illustrations of this research paper.

References

1. Rogers J, Morrison JH. Quantitative morphology and regional and laminar distributions of senile plaques in Alzheimer's disease. The Journal of neuroscience : the official journal of the Society for Neuroscience. 1985;5(10):2801-8.
2. Kawasaki H, Murayama S, Tomonaga M, Izumiyama N, Shimada H. Neurofibrillary tangles in human upper cervical ganglia. Morphological study with immunohistochemistry and electron microscopy. Acta neuropathologica. 1987;75(2):156-9.
3. Wisniewski HM, Kozlowski PB. Evidence for blood-brain barrier changes in senile dementia of the Alzheimer type (SDAT). Annals of the New York Academy of Sciences. 1982;396:119-29.
4. Krabbe G, Halle A, Matyash V, Rinnenthal JL, Eom GD, Bernhardt U, et al. Functional impairment of microglia coincides with Beta-amyloid deposition in mice with Alzheimer-like pathology. PloS one. 2013;8(4):e60921.
5. Crivelli SM, Giovagnoni C, Visseren L, Scheithauer AL, de Wit N, den Hoedt S, et al. Sphingolipids in Alzheimer's disease, how can we target them? Adv Drug Deliv Rev. 2020.
6. Hannun YA, Obeid LM. Principles of bioactive lipid signalling: lessons from sphingolipids. Nature reviews Molecular cell biology. 2008;9(2):139-50.
7. Zhang Y, Li X, Becker KA, Gulbins E. Ceramide-enriched membrane domains–structure and function. Biochimica et biophysica acta. 2009;1788(1):178-83.
8. Schwarz A, Futerman AH. Distinct roles for ceramide and glucosylceramide at different stages of neuronal growth. The Journal of neuroscience : the official journal of the Society for Neuroscience. 1997;17(9):2929-38.
9. Zhang H, Desai NN, Olivera A, Seki T, Brooker G, Spiegel S. Sphingosine-1-phosphate, a novel lipid, involved in cellular proliferation. The Journal of cell biology. 1991;114(1):155-67.
10. Bartke N, Hannun YA. Bioactive sphingolipids: metabolism and function. Journal of lipid research. 2009;50 Suppl:S91-6.
11. Perry DK, Hannun YA. The role of ceramide in cell signaling. Biochimica et biophysica acta. 1998;1436(1-2):233-43.
12. van Meer G, Holthuis JC. Sphingolipid transport in eukaryotic cells. Biochimica et biophysica acta. 2000;1486(1):145-70.
13. Cutler RG, Kelly J, Storie K, Pedersen WA, Tammara A, Hatanpaa K, et al. Involvement of oxidative stress-induced abnormalities in ceramide and cholesterol metabolism in brain aging and Alzheimer's

disease. Proceedings of the National Academy of Sciences of the United States of America. 2004;101(7):2070-5.

14. Mielke MM, Bandaru VV, Haughey NJ, Xia J, Fried LP, Yasar S, et al. Serum ceramides increase the risk of Alzheimer disease: the Women's Health and Aging Study II. Neurology. 2012;79(7):633-41.
15. He X, Huang Y, Li B, Gong CX, Schuchman EH. Deregulation of sphingolipid metabolism in Alzheimer's disease. Neurobiol Aging. 2010;31(3):398-408.
16. de Wit NM, Snkhchyan H, den Hoedt S, Wattimena D, de Vos R, Mulder MT, et al. Altered Sphingolipid Balance in Capillary Cerebral Amyloid Angiopathy. J Alzheimers Dis. 2016.
17. Fabelo N, Martin V, Marin R, Moreno D, Ferrer I, Diaz M. Altered lipid composition in cortical lipid rafts occurs at early stages of sporadic Alzheimer's disease and facilitates APP/BACE1 interactions. Neurobiology of aging. 2014;35(8):1801-12.
18. Puglielli L, Ellis BC, Saunders AJ, Kovacs DM. Ceramide stabilizes beta-site amyloid precursor protein-cleaving enzyme 1 and promotes amyloid beta-peptide biogenesis. The Journal of biological chemistry. 2003;278(22):19777–83.
19. Takasugi N, Sasaki T, Shinohara M, Iwatsubo T, Tomita T. Synthetic ceramide analogues increase amyloid-beta 42 production by modulating gamma-secretase activity. Biochem Biophys Res Commun. 2015;457(2):194-9.
20. Lee JT, Xu J, Lee JM, Ku G, Han X, Yang DI, et al. Amyloid-beta peptide induces oligodendrocyte death by activating the neutral sphingomyelinase-ceramide pathway. The Journal of cell biology. 2004;164(1):123-31.
21. Malaplate-Armand C, Florent-Bechard S, Youssef I, Koziel V, Sponne I, Kriem B, et al. Soluble oligomers of amyloid-beta peptide induce neuronal apoptosis by activating a cPLA2-dependent sphingomyelinase-ceramide pathway. Neurobiology of disease. 2006;23(1):178-89.
22. Hanada K, Kumagai K, Yasuda S, Miura Y, Kawano M, Fukasawa M, et al. Molecular machinery for non-vesicular trafficking of ceramide. Nature. 2003;426(6968):803-9.
23. Mencarelli C, Losen M, Hammels C, De Vry J, Hesselink MK, Steinbusch HW, et al. The ceramide transporter and the Goodpasture antigen binding protein: one protein--one function? J Neurochem. 2010;113(6):1369-86.
24. Crivelli SM, Paulus A, Markus J, Bauwens M, Berkes D, De Vries HE, et al. Synthesis, Radiosynthesis, and Preliminary in vitro and in vivo Evaluation of the Fluorinated Ceramide Trafficking Inhibitor (HPA-12) for Brain Applications. J Alzheimers Dis. 2017;60(3):783-94.
25. Wang X, Rao RP, Kosakowska-Cholody T, Masood MA, Southon E, Zhang H, et al. Mitochondrial degeneration and not apoptosis is the primary cause of embryonic lethality in ceramide transfer protein mutant mice. The Journal of cell biology. 2009;184(1):143-58.
26. Yasuda S, Kitagawa H, Ueno M, Ishitani H, Fukasawa M, Nishijima M, et al. A novel inhibitor of ceramide trafficking from the endoplasmic reticulum to the site of sphingomyelin synthesis. J Biol Chem. 2001;276(47):43994-4002.

27. Yamaji T, Hanada K. Establishment of HeLa cell mutants deficient in sphingolipid-related genes using TALENs. PLoS One. 2014;9(2):e88124.
28. Mencarelli C, Bode GH, Losen M, Kulharia M, Molenaar PC, Veerhuis R, et al. Goodpasture antigen-binding protein/ceramide transporter binds to human serum amyloid P-component and is present in brain amyloid plaques. J Biol Chem. 2012;287(18):14897-911.
29. Revert F, Ventura I, Martinez-Martinez P, Granero-Molto F, Revert-Ros F, Macias J, et al. Goodpasture antigen-binding protein is a soluble exportable protein that interacts with type IV collagen. Identification of novel membrane-bound isoforms. J Biol Chem. 2008;283(44):30246-55.
30. Bode GH, Losen M, Buurman WA, Veerhuis R, Molenaar PC, Steinbusch HW, et al. Complement activation by ceramide transporter proteins. Journal of immunology. 2014;192(3):1154-61.
31. Oakley H, Cole SL, Logan S, Maus E, Shao P, Craft J, et al. Intraneuronal β-Amyloid Aggregates, Neurodegeneration, and Neuron Loss in Transgenic Mice with Five Familial Alzheimer's Disease Mutations: Potential Factors in Amyloid Plaque Formation. The Journal of Neuroscience. 2006;26(40):10129-40.
32. Fluhrer R, Multhaup G, Schlicksupp A, Okochi M, Takeda M, Lammich S, et al. Identification of a beta-secretase activity, which truncates amyloid beta-peptide after its presenilin-dependent generation. J Biol Chem. 2003;278(8):5531-8.
33. Edelstein AD, Tsuchida MA, Amodaj N, Pinkard H, Vale RD, Stuurman N. Advanced methods of microscope control using μManager software. Journal of Biological Methods. 2014;1(2):e10.
34. House E, Collingwood J, Khan A, Korchazkina O, Berthon G, Exley C. Aluminium, iron, zinc and copper influence the in vitro formation of amyloid fibrils of A beta(42) in a manner which may have consequences for metal chelation therapy in Alzheimer's disease. Journal of Alzheimers Disease. 2004;6(3):291-301.
35. Mold M, Ouro-Gnao L, Wieckowski BM, Exley C. Copper prevents amyloid-beta(1-42) from forming amyloid fibrils under near-physiological conditions in vitro. Scientific reports. 2013;3:1256.
36. Kugler S, Lingor P, Scholl U, Zolotukhin S, Bahr M. Differential transgene expression in brain cells in vivo and in vitro from AAV-2 vectors with small transcriptional control units. Virology. 2003;311(1):89-95.
37. Verhaagen J, Hobo B, Ehlert EME, Eggers R, Korecka JA, Hoyng SA, et al. Small Scale Production of Recombinant Adeno-Associated Viral Vectors for Gene Delivery to the Nervous System. Methods Mol Biol. 2018;1715:3-17.
38. Franklin KB, Paxinos G, editors. The mouse brain in stereotaxic coordinates. San Diego, CA: Academic Press; 1997.
39. Prickaerts J, Moechars D, Cryns K, Lenaerts I, van Craenendonck H, Goris I, et al. Transgenic mice overexpressing glycogen synthase kinase 3beta: a putative model of hyperactivity and mania. The Journal of neuroscience : the official journal of the Society for Neuroscience. 2006;26(35):9022-9.
40. Sierksma AS, Prickaerts J, Chouliaras L, Rostamian S, Delbroek L, Rutten BP, et al. Behavioral and neurobiological effects of prenatal stress exposure in male and female APPswe/PS1dE9 mice.

Neurobiology of aging. 2013;34(1):319-37.

41. Mencarelli C, Bode GH, Losen M, Kulharia M, Molenaar PC, Veerhuis R, et al. Goodpasture antigen-binding protein/ceramide transporter binds to human serum amyloid P-component and is present in brain amyloid plaques. The Journal of biological chemistry. 2012;287(18):14897-911.
42. Young K, Morrison H. Quantifying Microglia Morphology from Photomicrographs of Immunohistochemistry Prepared Tissue Using ImageJ. J Vis Exp. 2018(136).
43. Blachnio-Zabielska AU, Persson XM, Koutsari C, Zabielski P, Jensen MD. A liquid chromatography/tandem mass spectrometry method for measuring the in vivo incorporation of plasma free fatty acids into intramyocellular ceramides in humans. Rapid Commun Mass Spectrom. 2012;26(9):1134-40.
44. Hoogendoorn A, den Hoedt S, Hartman EMJ, Krabbendam-Peters I, Te Lintel Hekkert M, van der Zee L, et al. Variation in Coronary Atherosclerosis Severity Related to a Distinct LDL (Low-Density Lipoprotein) Profile: Findings From a Familial Hypercholesterolemia Pig Model. Arterioscler Thromb Vasc Biol. 2019;39(11):2338-52.
45. Schmittgen TD, Livak KJ. Analyzing real-time PCR data by the comparative C(T) method. Nat Protoc. 2008;3(6):1101-8.
46. Gras SL, Waddington LJ, Goldie KN. Transmission electron microscopy of amyloid fibrils. Methods Mol Biol. 2011;752:197-214.
47. Oakley H, Cole SL, Logan S, Maus E, Shao P, Craft J, et al. Intraneuronal beta-amyloid aggregates, neurodegeneration, and neuron loss in transgenic mice with five familial Alzheimer's disease mutations: potential factors in amyloid plaque formation. The Journal of neuroscience : the official journal of the Society for Neuroscience. 2006;26(40):10129-40.
48. Ohno M, Cole SL, Yasvoina M, Zhao J, Citron M, Berry R, et al. BACE1 gene deletion prevents neuron loss and memory deficits in 5XFAD APP/PS1 transgenic mice. Neurobiology of disease. 2007;26(1):134-45.
49. Kimura R, Devi L, Ohno M. Partial reduction of BACE1 improves synaptic plasticity, recent and remote memories in Alzheimer's disease transgenic mice. Journal of neurochemistry. 2010;113(1):248-61.
50. Fukumoto H, Cheung BS, Hyman BT, Irizarry MC. Beta-secretase protein and activity are increased in the neocortex in Alzheimer disease. Arch Neurol. 2002;59(9):1381-9.
51. Matarin M, Salih DA, Yasvoina M, Cummings DM, Guelfi S, Liu W, et al. A genome-wide gene-expression analysis and database in transgenic mice during development of amyloid or tau pathology. Cell Rep. 2015;10(4):633-44.
52. Bandet CL, Mahfouz R, Veret J, Sotiropoulos A, Poirier M, Giussani P, et al. Ceramide Transporter CERT Is Involved in Muscle Insulin Signaling Defects Under Lipotoxic Conditions. Diabetes. 2018;67(7):1258-71.
53. Kumagai K, Yasuda S, Okemoto K, Nishijima M, Kobayashi S, Hanada K. CERT mediates intermembrane transfer of various molecular species of ceramides. J Biol Chem. 2005;280(8):6488-95.

54. De Strooper B, Annaert W. Proteolytic processing and cell biological functions of the amyloid precursor protein. Journal of cell science. 2000;113 (Pt 11):1857-70.
55. Girard SD, Jacquet M, Baranger K, Migliorati M, Escoffier G, Bernard A, et al. Onset of hippocampus-dependent memory impairments in 5XFAD transgenic mouse model of Alzheimer's disease. Hippocampus. 2014;24(7):762-72.
56. Savage JC, Jay T, Goduni E, Quigley C, Mariani MM, Malm T, et al. Nuclear receptors license phagocytosis by trem2+ myeloid cells in mouse models of Alzheimer's disease. The Journal of neuroscience : the official journal of the Society for Neuroscience. 2015;35(16):6532-43.
57. Kanazawa H, Ohsawa K, Sasaki Y, Kohsaka S, Imai Y. Macrophage/microglia-specific protein Iba1 enhances membrane ruffling and Rac activation via phospholipase C-gamma -dependent pathway. J Biol Chem. 2002;277(22):20026-32.
58. Olabarria M, Noristani HN, Verkhratsky A, Rodriguez JJ. Concomitant astroglial atrophy and astrogliosis in a triple transgenic animal model of Alzheimer's disease. Glia. 2010;58(7):831-8.
59. Dinkins MB, Enasko J, Hernandez C, Wang G, Kong J, Helwa I, et al. Neutral Sphingomyelinase-2 Deficiency Ameliorates Alzheimer's Disease Pathology and Improves Cognition in the 5XFAD Mouse. The Journal of neuroscience : the official journal of the Society for Neuroscience. 2016;36(33):8653-67.
60. Beher D, Hesse L, Masters CL, Multhaup G. Regulation of amyloid protein precursor (APP) binding to collagen and mapping of the binding sites on APP and collagen type I. J Biol Chem. 1996;271(3):1613-20.
61. Multhaup G. Identification and regulation of the high affinity binding site of the Alzheimer's disease amyloid protein precursor (APP) to glycosaminoglycans. Biochimie. 1994;76(3-4):304-11.
62. Breen KC, Bruce M, Anderton BH. Beta amyloid precursor protein mediates neuronal cell-cell and cell-surface adhesion. J Neurosci Res. 1991;28(1):90-100.
63. Turner N, Mason PJ, Brown R, Fox M, Povey S, Rees A, et al. Molecular cloning of the human Goodpasture antigen demonstrates it to be the alpha 3 chain of type IV collagen. J Clin Invest. 1992;89(2):592-601.
64. Verdier Y, Zarandi M, Penke B. Amyloid beta-peptide interactions with neuronal and glial cell plasma membrane: binding sites and implications for Alzheimer's disease. J Pept Sci. 2004;10(5):229-48.
65. Ebel P, Vom Dorp K, Petrasch-Parwez E, Zlomuzica A, Kinugawa K, Mariani J, et al. Inactivation of ceramide synthase 6 in mice results in an altered sphingolipid metabolism and behavioral abnormalities. J Biol Chem. 2013;288(29):21433-47.
66. Imgrund S, Hartmann D, Farwanah H, Eckhardt M, Sandhoff R, Degen J, et al. Adult ceramide synthase 2 (CERS2)-deficient mice exhibit myelin sheath defects, cerebellar degeneration, and hepatocarcinomas. J Biol Chem. 2009;284(48):33549-60.
67. Salegio EA, Samaranch L, Jenkins RW, Clarke CJ, Lamarre C, Beyer J, et al. Safety study of adeno-associated virus serotype 2-mediated human acid sphingomyelinase expression in the nonhuman primate brain. Hum Gene Ther. 2012;23(8):891-902.

68. Flanigan TJ, Xue Y, Kishan Rao S, Dhanushkodi A, McDonald MP. Abnormal vibrissa-related behavior and loss of barrel field inhibitory neurons in 5xFAD transgenics. Genes Brain Behav. 2014;13(5):488-500.
69. Jawhar S, Trawicka A, Jenneckens C, Bayer TA, Wirths O. Motor deficits, neuron loss, and reduced anxiety coinciding with axonal degeneration and intraneuronal Abeta aggregation in the 5XFAD mouse model of Alzheimer's disease. Neurobiology of aging. 2012;33(1):196 e29-40.
70. Katsel P, Li C, Haroutunian V. Gene expression alterations in the sphingolipid metabolism pathways during progression of dementia and Alzheimer's disease: a shift toward ceramide accumulation at the earliest recognizable stages of Alzheimer's disease? Neurochem Res. 2007;32(4-5):845-56.
71. Couttas TA, Kain N, Tran C, Chatterton Z, Kwok JB, Don AS. Age-Dependent Changes to Sphingolipid Balance in the Human Hippocampus are Gender-Specific and May Sensitize to Neurodegeneration. J Alzheimers Dis. 2018;63(2):503-14.
72. Han X, D MH, McKeel DW, Jr., Kelley J, Morris JC. Substantial sulfatide deficiency and ceramide elevation in very early Alzheimer's disease: potential role in disease pathogenesis. J Neurochem. 2002;82(4):809-18.
73. Barrier L, Fauconneau B, Noel A, Ingrand S. Ceramide and Related-Sphingolipid Levels Are Not Altered in Disease-Associated Brain Regions of APP and APP/PS1 Mouse Models of Alzheimer's Disease: Relationship with the Lack of Neurodegeneration? Int J Alzheimers Dis. 2010;2011:920958.
74. Thinakaran G, Koo EH. Amyloid precursor protein trafficking, processing, and function. J Biol Chem. 2008;283(44):29615-9.
75. Lopez-Montero I, Rodriguez N, Cribier S, Pohl A, Velez M, Devaux PF. Rapid transbilayer movement of ceramides in phospholipid vesicles and in human erythrocytes. J Biol Chem. 2005;280(27):25811-9.
76. Silva L, de Almeida RF, Fedorov A, Matos AP, Prieto M. Ceramide-platform formation and -induced biophysical changes in a fluid phospholipid membrane. Mol Membr Biol. 2006;23(2):137-48.
77. Heppner FL, Ransohoff RM, Becher B. Immune attack: the role of inflammation in Alzheimer disease. Nature reviews Neuroscience. 2015;16(6):358-72.
78. Jonsson T, Stefansson H, Steinberg S, Jonsdottir I, Jonsson PV, Snaedal J, et al. Variant of TREM2 associated with the risk of Alzheimer's disease. The New England journal of medicine. 2013;368(2):107-16.
79. Wood JA, Wood PL, Ryan R, Graff-Radford NR, Pilapil C, Robitaille Y, et al. Cytokine indices in Alzheimer's temporal cortex: no changes in mature IL-1β or IL-1RA but increases in the associated acute phase proteins IL-6, α2-macroglobulin and C-reactive protein. Brain Research. 1993;629(2):245-52.
80. Cojocaru IM, Cojocaru M, Miu G, Sapira V. Study of interleukin-6 production in Alzheimer's disease. Romanian journal of internal medicine = Revue roumaine de medecine interne. 2011;49(1):55-8.
81. Hull M, Fiebich BL, Lieb K, Strauss S, Berger SS, Volk B, et al. Interleukin-6-associated inflammatory processes in Alzheimer's disease: new therapeutic options. Neurobiology of aging. 1996;17(5):795-800.

82. Angelis P, Scharf S, Mander A, Vajda F, Christophidis N. Serum interleukin-6 and interleukin-6 soluble receptor in Alzheimer's disease. Neuroscience letters. 1998;244(2):106-8.
83. Wang G, Dinkins M, He Q, Zhu G, Poirier C, Campbell A, et al. Astrocytes secrete exosomes enriched with proapoptotic ceramide and prostate apoptosis response 4 (PAR-4): potential mechanism of apoptosis induction in Alzheimer disease (AD). J Biol Chem. 2012;287(25):21384-95.
84. Dinkins MB, Dasgupta S, Wang G, Zhu G, Bieberich E. Exosome reduction in vivo is associated with lower amyloid plaque load in the 5XFAD mouse model of Alzheimer's disease. Neurobiology of aging. 2014;35(8):1792-800.
85. de Wit NM, den Hoedt S, Martinez-Martinez P, Rozemuller AJ, Mulder MT, de Vries HE. Astrocytic ceramide as possible indicator of neuroinflammation. J Neuroinflammation. 2019;16(1):48.
86. Elsherbini A, Kirov AS, Dinkins MB, Wang G, Qin H, Zhu Z, et al. Association of Abeta with ceramide-enriched astrosomes mediates Abeta neurotoxicity. Acta Neuropathol Commun. 2020;8(1):60.
87. Buchhalter JR, Dichter MA. Electrophysiological comparison of pyramidal and stellate nonpyramidal neurons in dissociated cell culture of rat hippocampus. Brain Res Bull. 1991;26(3):333-8.
88. Youmans KL, Tai LM, Nwabuisi-Heath E, Jungbauer L, Kanekiyo T, Gan M, et al. APOE4-specific changes in Abeta accumulation in a new transgenic mouse model of Alzheimer disease. J Biol Chem. 2012;287(50):41774-86.

Figures

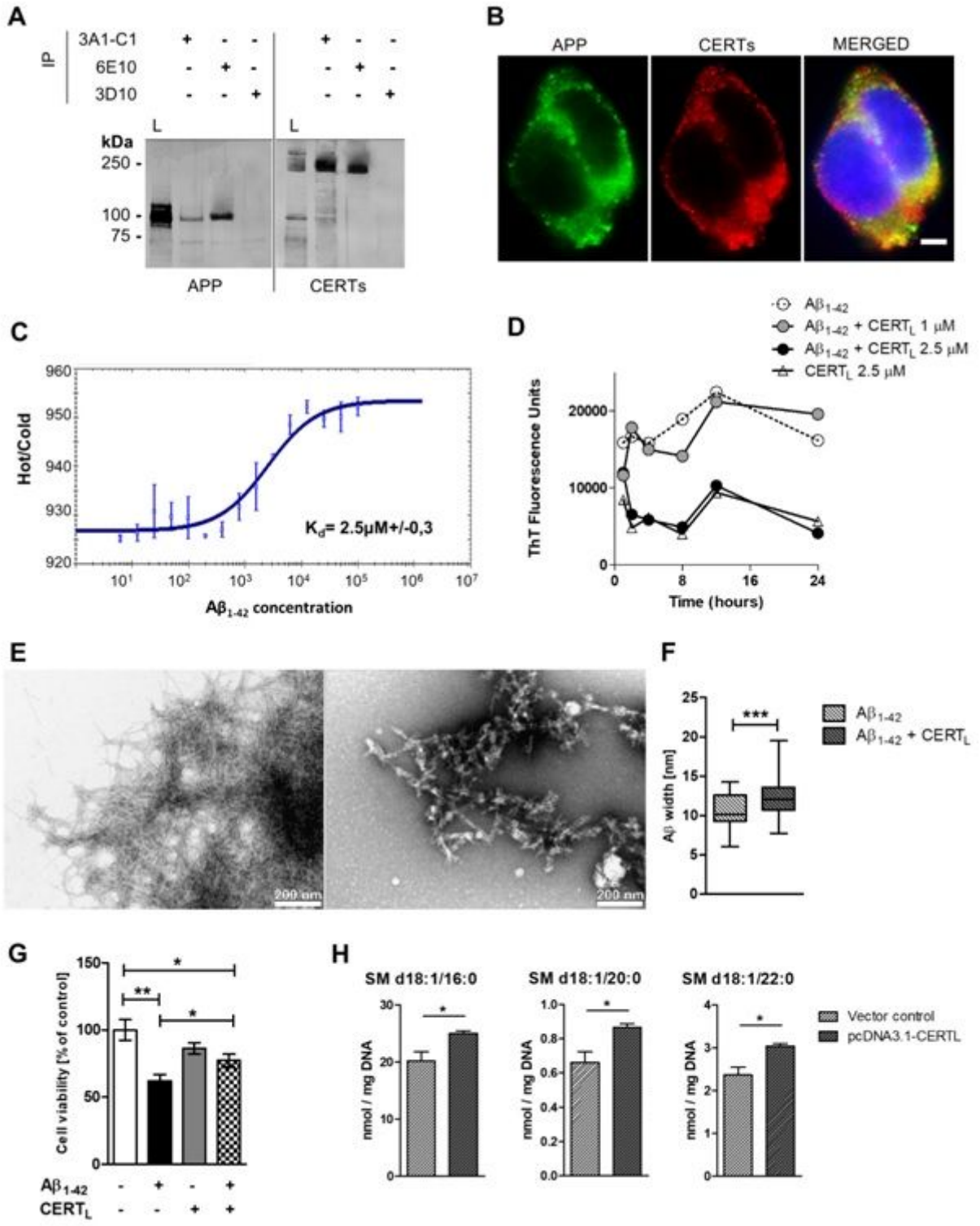

Figure 1

CERTL binds directly to APP and Aβ, and reduces Aβ aggregation and toxicity in vitro. A) Protein interaction detected using co-IP of APP and CERTL in HEK-APP. The total cell lysate of HEK-APP cells (L) lane 1 and the total cell lysate of HEK-APP cells IP using APP (6E10) (lane 2), CERTL (lane 3) and syntaxin (isotype control) (lane 4) antibodies were analyzed by Western blot. APP (1) and CERTs proteins were detected. Molecular weight markers are indicated (kDa).B) Immunofluorescent staining showing co-

localization of CERTs and APP in HEK-APP cells. DAPI was used for nuclei staining. Scale bar10µm. C) CERTLand Aβ1-42interaction was measure bymicroscale thermophoresis.The dissociation constant (Kd) calculated was2.5+/-0.3 µM.D)Measurement of ThioflavinT (ThT) fluorescence intensity to detect Aβ1-42 aggregation in the absence or presence of recombinant CERTLat different time points. Each data point represents the mean fluorescent intensity of three wells. E and F) TEM analysis of Aβ1-42 aggregation in the absence and presence of CERTL showed a different aggregation pattern quantified by Aβ width (student's t-test ***p<0.001). G) Measurement of cell metabolic activity of SH-SY5Y by MTT assay incells incubated with medium alone (control) or medium containing Aβ1-42, Aβ1-42,and CERTL, or CERTLalone for 24 hours. Graph bar expressed as means ± S.E.M % of control N= 5-10 (one-way ANOVA, Bonferroni correction *p< 0.05; **p<0.01). H) SM d18:1/16:0, SM d18:1/20:0 and SM d18:1/22:0 measured by HPLC-MS/MSin HEK cells after 72 hours transfection with vector control or pcDNA-CERTL. Graph bar expressed as means ± S.E.M % of control N= 3 / group (student's t-test *p<0.05)

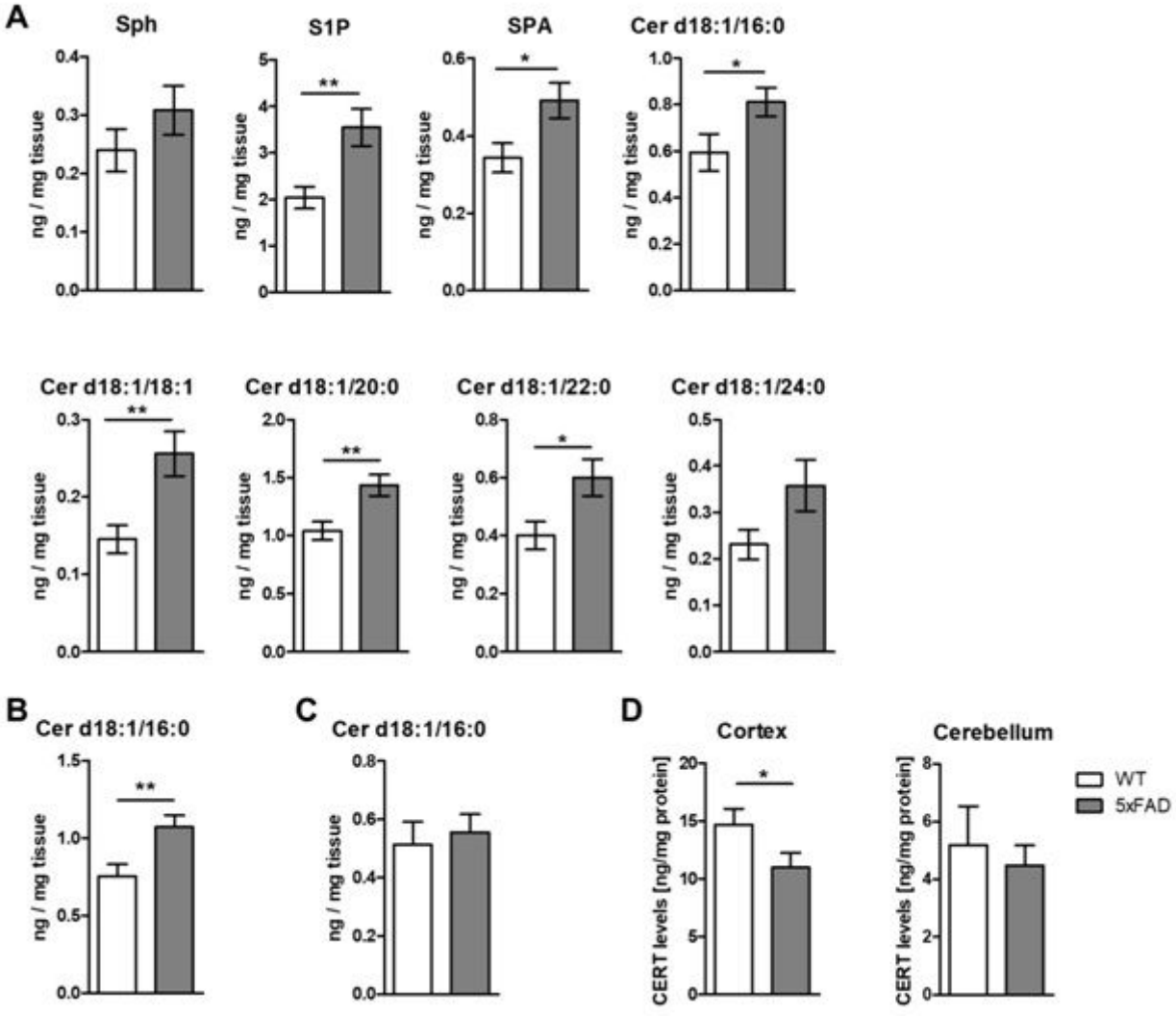

Figure 2

Ceramide levels are increased in 5xFAD compared to WT animals depending on brain region and acyl chain length while CERT levels are reduced.Sphingolipids levels were measured in the hippocampus (A), cortex (B), and cerebellum (C) by HPLC-MS/MS of WT and 5xFAD mice. Sphingolipids were classified

based on acyl chain number of carbons (Sph, S1P, SPA, Cer d18:1/16:0, Cer d18:1/18:1, Cer d18:1/20:0, Cer d18:1/22:0 and Cer d18:1/24:0). CERT was quantified by ELISA in protein extract of cortex and cerebellum of WT and 5xFAD animals. Bars represent the mean ± S.E.M per group N=11-12 (student's t-test *p<0.05; **p<0.01).

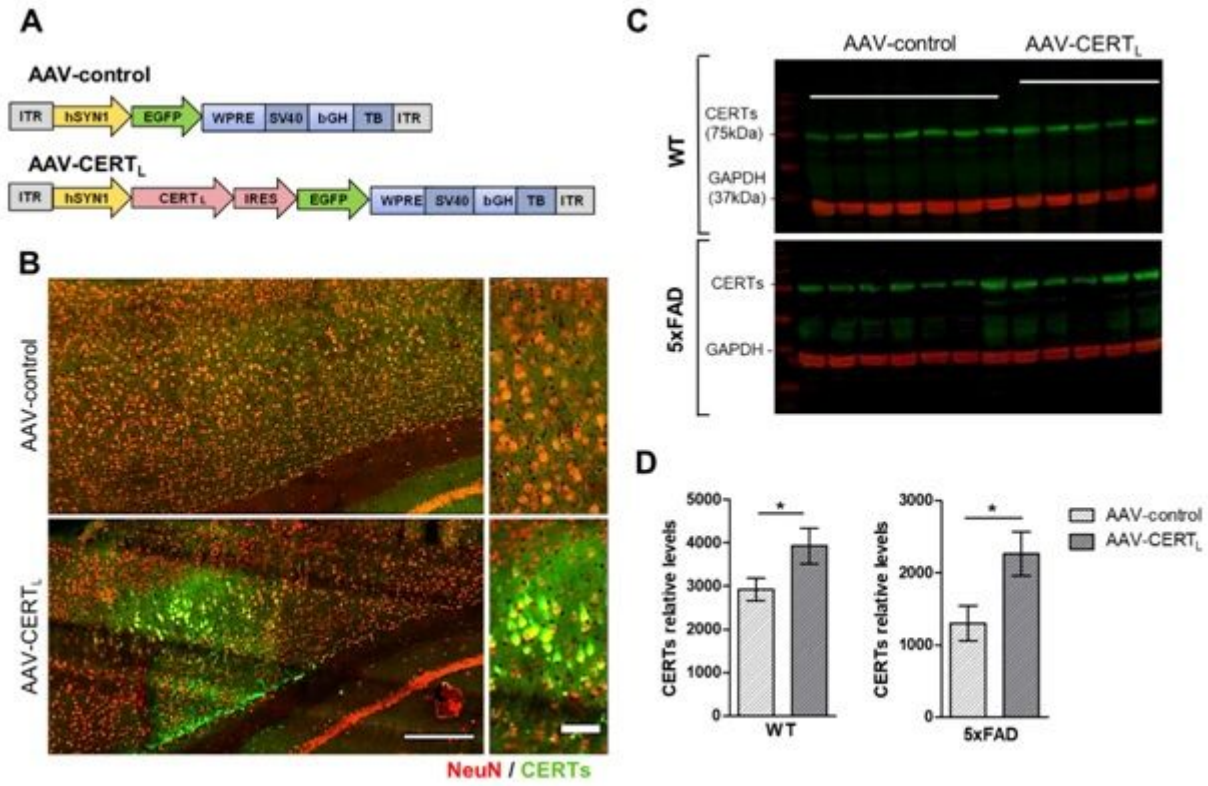

Figure 3

AAV-mediated neuronal expression of CERTL in mouse brain. A) The recombinant genomes of the two AAV-2 vectors. Abbreviations: From left to right, ITR, inverted terminal repeats; hSYN1, human synapsin 1 gene promoter; CERTL, cDNA sequence coding for ceramide transfer protein long isoform (hCERTL, 1875bp NP_005704.1); IRES internal ribosome sequence for translation initiation. EGFP, cDNA coding for enhanced green fluorescent protein; GFP; WPRE, woodchuck hepatitis virus posttranscriptional control element; bGH, bovine growth hormone gene-derived polyadenylation site; TB, synthetic transcription blocker. B) Representative images of immunofluorescent staining of cortical brain area from 5xFAD animals treated with AAV-controlor AAV-CERTL. Section was co-stain for CERTs protein (green), neuronal marker NeuN (red). Scale bar 200 µM and 50µM. C) Western blot showing band intensities of CERTs and GAPDH. D) Relative quantification of CERTs levels normalized to GAPDH in cortical protein extract from WT and 5xFAD animals treated with AAV-controlor AAV-CERTL. Bars represent mean one representative experiment with 5-7 samplespergroup (Mann Whitney test, * p<0.05).

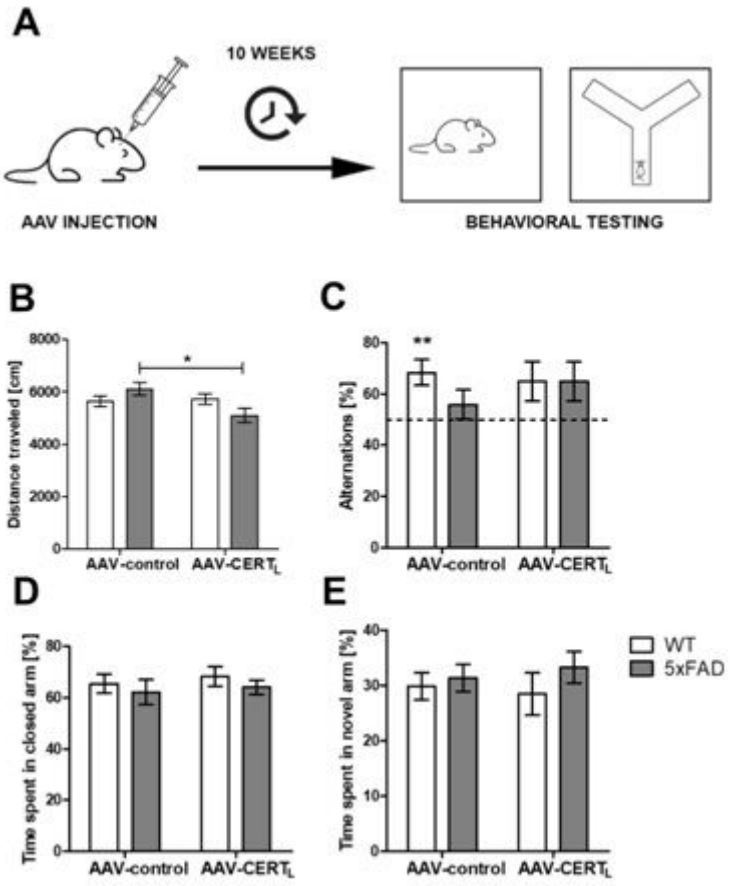

Figure 4

No behavioral abnormalities 10 weeks after injection of AAV-CERTL. A) The effects of CERTL over-expression were investigated in 30 5xFAD and 30 WT males. Mice were bilaterally injected at 12-13 weeks of age with AAV-CERTLor AAV-control particles at the dose 1.12*10E8 transducing unit (t.u.). Starting at week 22 of age,animals were challenged with the following behavioral tests: Open Field (OF) for locomotion activity, Alternate Y-Maze (AYM), and Spatial Y-Maze (SYM) for spatial memory and Elevated Zero Maze (EZM) for anxiety. B) Locomotion expressed as distance traveled in OF task. C) The graph shows the results of the working memory in the AYMtask as a percentage of correct alternation in the first four triads. Percentage were compared to 50% chance levels (one sample t-test **p<0.01). D) Anxiety was assessed,measuring the percentage of time spent in the closed arm in EZM. E) Memory was measured in SYM expressed as a percentage of time spent in the novel arm.(Bars represent the means ± S.E.M per group N=10-20 (two-way ANOVA, interaction effect F=4.170 p=0.0463, LSD, *p < 0.05).

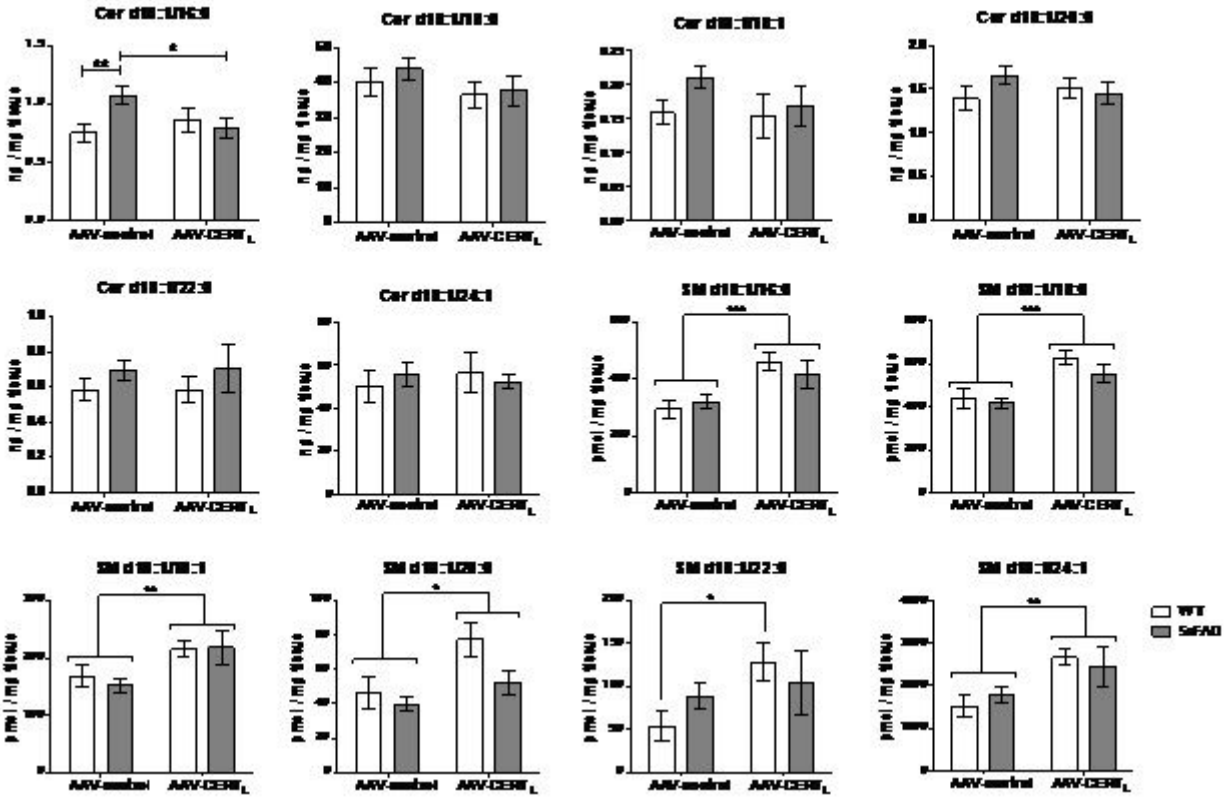

Figure 5

AAV-CERTL reduces Cer d18:1/16:0 and increases sphingomyelin species in the cortex. Sphingolipids levels were measured in the cortex by HPLC-MS/MS. Ceramides were classified based on acyl chain number of carbons (Cer d18:1/16:0, Cer d18:1/18:0, Cer d18:1/18:1, Cer d18:1/20:0, Cer d18:1/22:0 and Cer d18:1/24:1). as well as sphingomyelin (SM d18:1/16:0, SM d18:1/18:0, SM d18:1/18:1, SM d18:1/20:0, SM d18:1/22:0 and SM d18:1/24:1). Ceramides levels were expressed as ng/mg tissue, while sphingomyelins were expressed as pmol/mg tissue. Bars represent the mean ± S.E.M per group N=5-12 (two-way ANOVA, LSD, significant effects, *p< 0.05; **p<0.01; ***p<0.001).

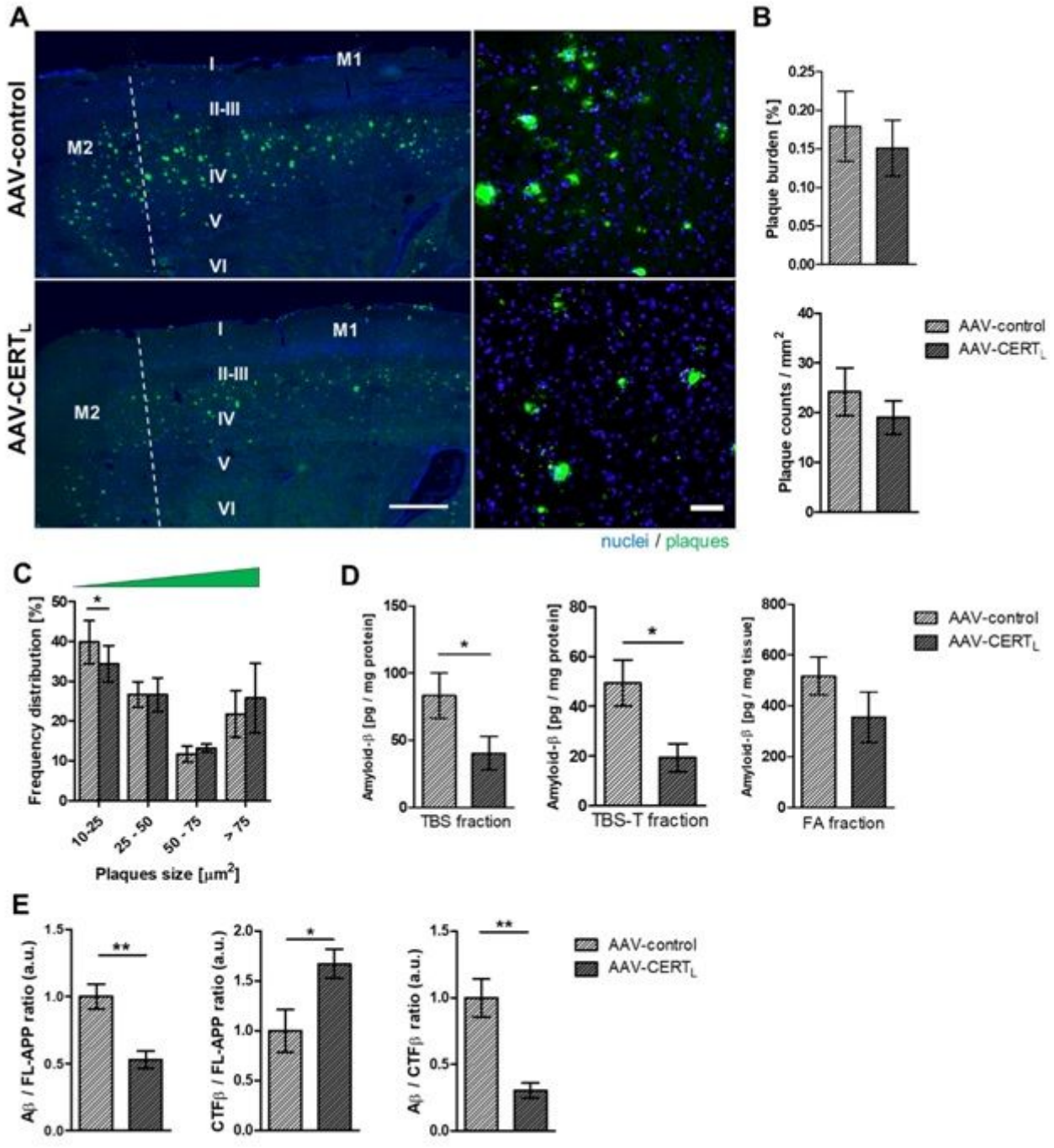

Figure 6

Neuronal increase of CERTL reduces Aβ by decreasing APP cleavage. A) Representative photomicrographs of sagittal brain sections imaging the motor sensory cortex (M1 and M2) stained for nuclei in blue and Aβ plaques in green. All photomicrographs were exposed and processed identically. Scale bar represents 200 and 50 μm (from right to left). B) Immunofluorescent quantification of plaques measured by the percentage of area, plaques counts / mm2. C) Frequency distribution of plaques based on size (10-25 μm) (Errors bars represent +/- SEM of 4-6 animals per experimental condition, ANOVA, Bonferroni correction, significant effects, *p< 0.05; **p<0.01). D) Aβ quantification in three extraction buffers, BS, TBS-T, and formic acid (FA) by ELISA showed that Aβ was significantly reduced in the soluble

fractions in the cortex but not in the insoluble fraction (student's t-test *p<0.05). E) Western blot analysis of TBS cortex homogenate stained with 6E10 antibody showed that ratios of amyloid Aβ /FL-APP and Aβ/ CTFβ are reduced while CTFβ / FL-APP is increased in AAV-CERTL treated animals while CTFβ / FL-APPis increased. Errors bars represent +/- SEM of 5 animals per experimental condition (student's t-test *p<0.05; **p<0.01). (Full length amyloid precursor protein = FL-APP; amyloid-β peptide = Aβ; C-terminal fragment β = CFTβ). Western blot membranes are shown in Supplementary figure 5.

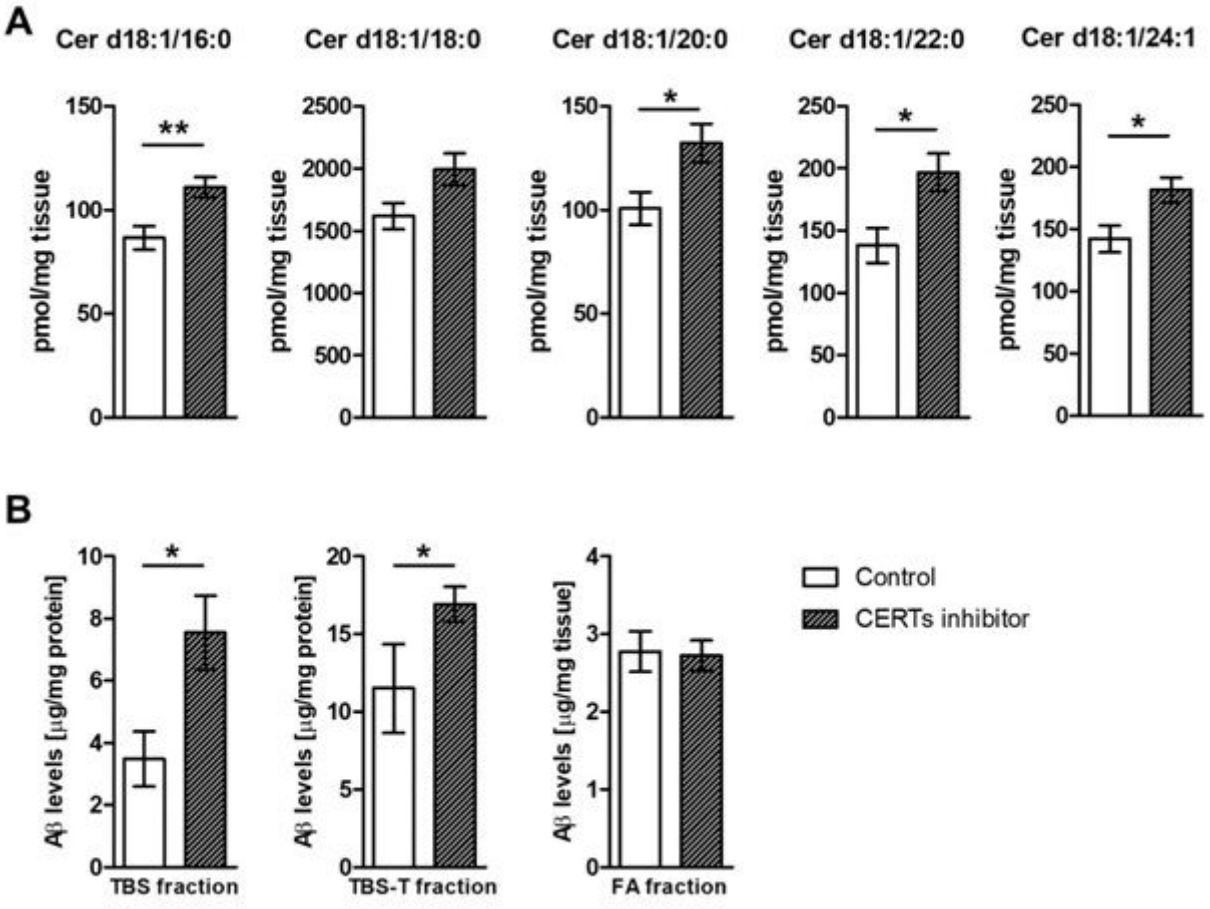

Figure 7

CERTs inhibitor increasesCer andAβ levels in the brain of transgenic AD mice.A) Sphingolipids levels were measured in the cortex by HPLC-MS/MS. Ceramides were classified based on acyl chain number of carbons (Cer d18:1/16:0, Cer d18:1/18:0, Cer d18:1/22:0 and Cer d18:1/24:1) and levels were expressed as pmol / mg tissue. Bars represent the mean ± S.E.M per group N=10-12 (student's t-test *p<0.05)Aβ quantification in hippocampus homogenate extracted in three buffers, TBS, TBS-T and formic acid (FA) by enzyme-linked immunoassays.Means of each fraction were compared with unpaired t-test (Control N=10; HPA-12 N=13; *p<0.05)

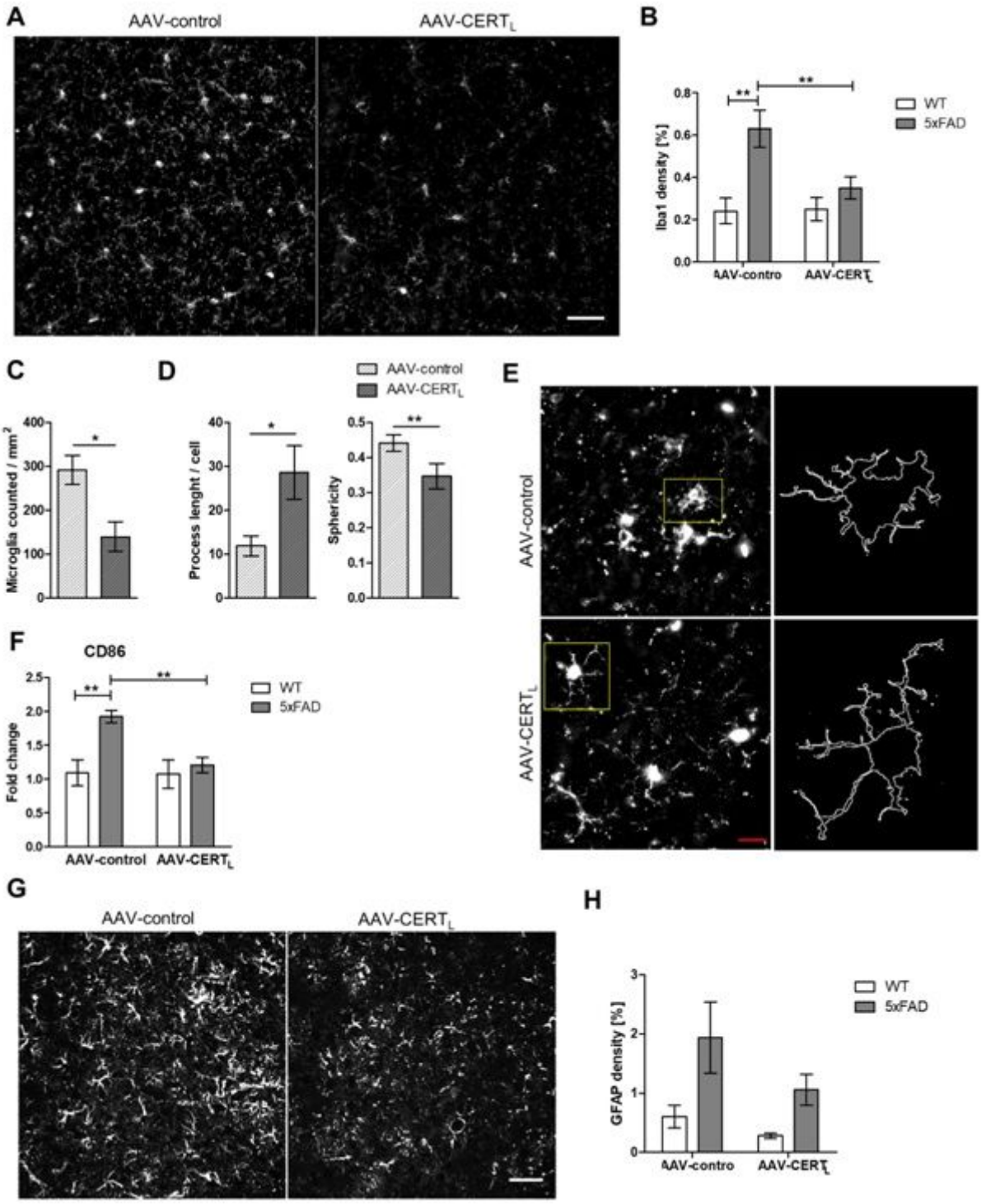

Figure 8

AAV-CERTL reduces microglia reactivity to Iba1 and CD86 expression levels but has no significant effect on GFAP immunoreactivity in the cortex of 5xFAD mice. A)Representative photomicrograph of Iba1 staining in the cortical motor sensory region of 5xFAD animals treated with AAV-control or AAV-CERTL (Scale bar 50µm). B) Densitometric analysis of Iba1 stainingrepresented as a percentage of the area (AAV-control n=6 and AAV-CERTL n=4 for WT and 5xFAD groups). C) Densitometric analysis of Iba1 stainingrepresented as number of positive Iba1 cells / mm2 (AAV-control n=6 and AAV-CERTL n=4 for

5xFAD groups).D) Length of microglia ramification and sphericity per cell inAAV-control or AAV-CERTL. Morphological analysis was performed on 3-5 pictures/group. E) Illustrations of the microglia morphological analysis applied to a fluorescent photomicrograph captured with 60x objective with a single cell cropped to show details. Scale bar = 20. F) Analysis of gene expression of membrane markers CD86(4-5 number of animals per group).G) Representative photomicrographs of GFAP staining in the cortical motor sensory region of 5xFAD animals treated with AAV-control or AAV-CERTL (Scale bar 50µm). H) Densitometric analysis of GFAP staining represented as a percentage of the area(AAV-control n=6 and AAV-CERTL n= 4 for WT and 5xFAD groups). Bars represent the mean ± S.E.M per group(two-way ANOVA, LSD, significant effects, *p< 0.05; **p<0.01; ***p<0.001).

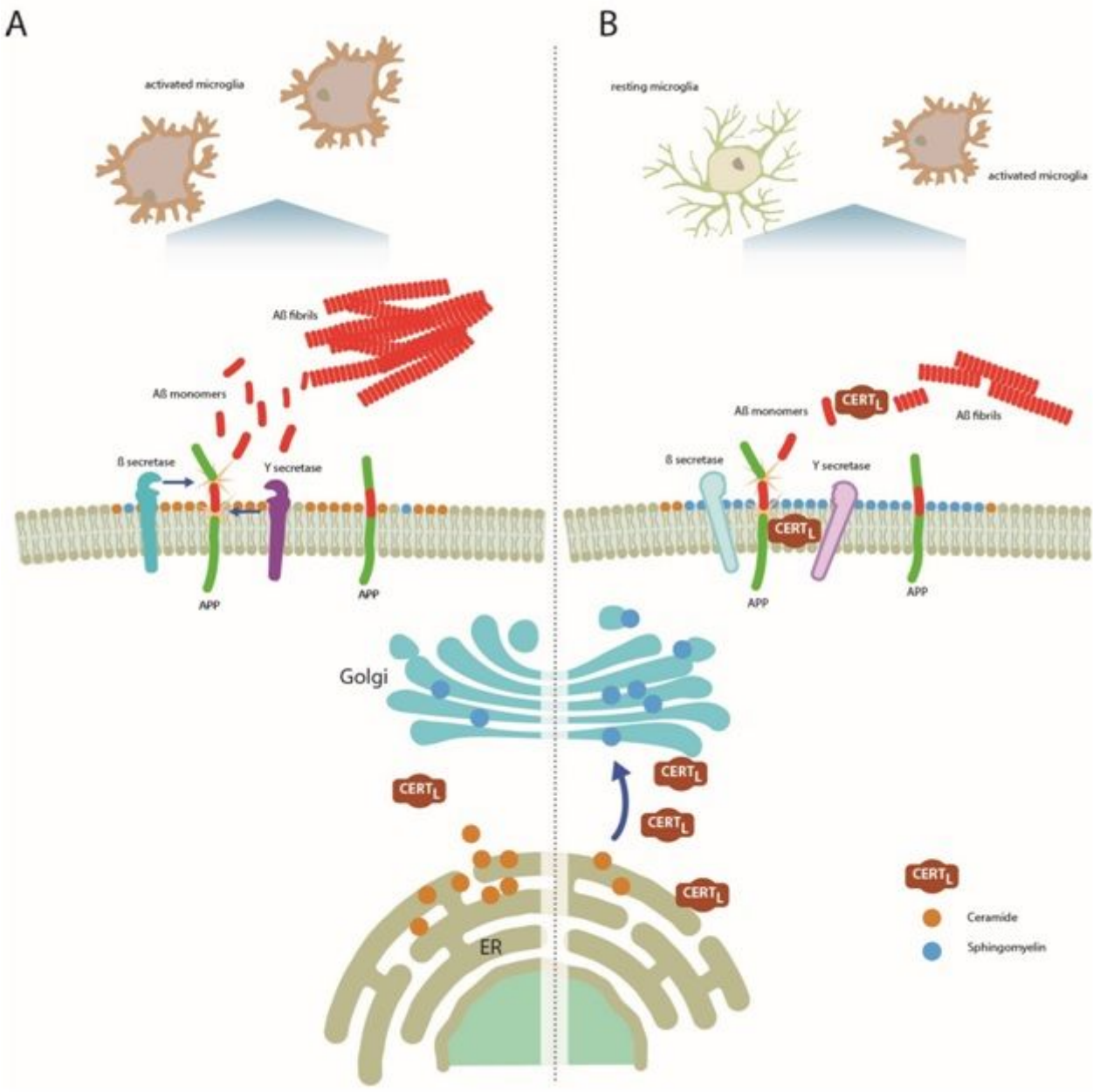

Figure 9

Schematic model of CERTL action in AD. A) CERTLconcentration is decreased in AD neuronal cells. Consequently, the transport of Cer to the Golgi is impaired and Cer accumulates in the cell. Cer elevation

stabilizes and favors the secretases activity. The amyloidogenic APP processing is favored and Aβ is produced. The neighboring microglia changes the resting status to activate. B) By overexpressing CERTLthe physiological transfer of Cer from the ER to the Golgi is restored favoring SM synthesis, which is intensified. The reduction of Cer levels in neuronal cells diminished secretases activity, reducing Aβ biogenesis. The interaction between CERTL and APP may be important in stabilizing APP in the membrane and in protecting APP from secretase activity. Furthermore, CERTL affects Aβ fibrilization by organizing Aβ into less neurotoxic aggregates that may be cleared from the brain more easily and reduces the number of activated microglia.

Supplementary Files

This is a list of supplementary files associated with this preprint. Click to download.

- supplDoc.docx